laval Research Laboratory
ashington, DC 20375-5320

NRL/MR/6793--93-7183

New Results and Applications for the Quasioptical Gyrotron

ARNE W. FLIFLET
RICHARD P. FISCHER
WALLACE M. MANHEIMER

Beam Physics Branch
Plasma Physics Division

February 26, 1993

REPORT DOCUMENTATION PAGE

Form Approved
OMB No. 0704-0188

1. AGENCY USE ONLY (*Leave Blank*)	2. REPORT DATE	3. REPORT TYPE AND DATES COVERED
	February 26, 1993	Interim

4. TITLE AND SUBTITLE

New Results and Applications for the Quasioptical Gyrotron

5. FUNDING NUMBERS

JO-673046-03

6. AUTHOR(S)

A.W. Fliflet, R.P. Fischer and
W.M. Manheimer

7. PERFORMING ORGANIZATION NAME(S) and ADDRESS(ES)

Naval Research Laboratory
Washington, DC 20375-5320

8. PERFORMING ORGANIZATION REPORT NUMBER

NRL/MR/6793--93-7183

9. SPONSORING/MONITORING AGENCY NAME(S) AND ADDRESS(ES)

Office of Naval Research
Arlington, VA 22217

10. SPONSORING/MONITORING AGENCY REPORT NUMBER

11. SUPPLEMENTARY NOTES

12a. DISTRIBUTION/AVAILABILITY STATEMENT

Approved for public release; distribution unlimited.

12b. DISTRIBUTION CODE

13. ABSTRACT (*Maximum 200 words*)

The quasioptical gyrotron (QOG), which features an open resonator formed by a pair of spherical mirrors instead of the conventional gyrotron waveguide cavity, has been under development at the U.S. Naval Research Laboratory as a tunable high power millimeterwave source for tokamak plasma heating, advanced radars, and power beaming. In the free running oscillator configuration, the QOG has produced a peak power of 600kW at a frequency of 120GHZ, and a peak efficiency of 12% at 200kW. Results have recently been obtained for a quasioptical gyroklystron (QOGK) realized by the addition of an open-mirror prebunching resonator driven by an 85GHz, 1.5kW Extended Interaction Oscillator. Efficiency enhancement by mode priming has been investigated, and efficiencies up to 19% have been obtained by increasing the detuning of the operating mode. An overall efficiency of 30% was obtained by the addition of a simple depressed collector. The high circulating power in the QOG resonator is currently being considered for use as an electromagnetic wiggler for compact IR free-electron lasers. The QOG is also promising as a source for an active sensor of upper atmosphere trace impurities.

14. SUBJECT TERMS

Gyrotrons
Quasioptical gyrotron
Free-electron laser
Gyroklystron
Electromagnetic wiggler
Atmospheric sensing

15. NUMBER OF PAGES

50

16. PRICE CODE

17. SECURITY CLASSIFICATION OF REPORT	18. SECURITY CLASSIFICATION OF THIS PAGE	19. SECURITY CLASSIFICATION OF ABSTRACT	20. LIMITATION OF ABSTRACT
UNCLASSIFIED	UNCLASSIFIED	UNCLASSIFIED	UL

NSN 7540-01-280-5500

Standard Form 298 (Rev. 2-89)
Prescribed by ANSI Std 239-18
298-102

CONTENTS

I. Introduction 1

II. Experimental Results 5

III. QOG Wiggler FEL 12

IV. Remote Sensing of Upper Atmospheric Impurities 22

V. Acknowledgements and References 27

I Introduction

Electron cyclotron resonance masers with waveguide cavities, usually called gyrotrons, are well established as the leading source of coherent, high average power millimeter-wave radiation. Developed primarily as a source for electron cyclotron heating of tokomak plasmas, gyrotrons have achieved megawatt peak powers, and average powers of several hundred kilowatts, at frequencies above 100 GHz. However, as waveguide cavity gyrotrons are driven to higher frequencies and power levels, a number of major obstacles arise. These include, among others, wall heating, mode competition, and collection of the spent electron beam. The quasioptical gyrotron (QOG) configuration was introduced in order to overcome many of the limitations generic to conventional gyrotrons. The QOG was first proposed and analyzed in 1980 by Sprangle, Vomvoridis, and Manheimer[1] at the Naval Research Laboratory (NRL). The development of QOGs to date has been driven by the need for sources for rf heating of tokamak plasmas. However, there are other applications for which the QOG seems especially well-suited. Two of these new applications are discussed in this paper, namely, it's use as i) an electromagnetic wiggler for a compact IR FEL, and ii) a tunable, high power millimeter-wave source for sensing of upper atmosphere trace impurities.

The QOG is based on an electron cyclotron interaction as are the gyrotrons and cyclotron autoresonance masers (CARMs), but it utilizes an open Fabry-Perot type resonator instead of a closed cavity configuration. The basic structure of the quasi-optical gyrotron, shown in Figure 1, consists of one or more open resonators which are traversed by a beam of gyrating electrons guided by an applied magnetic field. In the simplest configuration each resonator consists of a pair of appropriately curved mirrors. Both the waveguide cavity gyrotron and the QOG have the advantage that they can operate efficiently at low voltages (<100 keV). Low voltage operation allows for more compact and less expensive power supplies, and reduces the amount of x-ray shielding required. The inherent separation of the electron and radiation beams in the QOG facilitates output coupling and the use of a depressed collector for spent beam energy recovery. Since the QOG utilizes an open resonator and thus can have a large interaction volume, the input electron beam power can be extremely high while the

Manuscript approved January 22, 1993.

power density can be kept fairly low. The usual limitations on beam power imposed by space charge effects can therefore be substantially eliminated. The wave–particle interaction can be efficient, similar to the conventional gyrotron. Efficient coupling between the electrons and radiation field can occur near harmonics of the relativistic cyclotron frequency allowing harmonic operation. In addition, the operating frequency is limited solely by the external magnetic field and is independent of the dimensions of any physical structure. This leads to a capability for wide, continuous tunability.

There is by now a considerable data base on the main features of the QOG obtained, for the most part, in experimental programs at NRL and the Center for Research on Plasma Physics (CRPP), Ecole Polytechnique in Lausanne, Switzerland[2]—[10]. However, the industrial development and utilization of QOGs in tokamak experiments has lagged for several reasons. Firstly, the demonstrated peak output efficiency of the QOG has been $\sim 12\%$, which is significantly less than the $> 40\%$ efficiency achieved by waveguide cavity gyrotrons. Somewhat lower efficiencies are expected for the QOG, due to electron beam geometry and mode competion effects, but until recently, the observed efficiencies have been less than half the predicted values. Secondly, the problem of obtaining a pure output mode, which is needed for low-loss power transmission, has been a concern. Finally, the QOG usually requires a "cold-bore" superconducting magnet configuration, which complicates the usual processing required by high average power microwave tubes. Significant progress has been made on efficiency enhancement during the past year at NRL, with the demonstration of single-moded operation of the QOG with an electronic efficiency of 19%. The overall efficiency was increased to 30% with a simple depressed collector. In addition, the demonstration of a QOG with a gaussian mode output at CRPP represents a major advance in output coupler design[11]. A discussion of the new efficiency results is a major topic of this paper. It is anticipated that these promising results will stimulate progress in the engineering of QOGs for high average power using techniques developed for the assembly of high average power RF accelerators.

Progress in efficiency enhancement has come as the result of experiments on a quasioptical gyroklystron (QOGK) configuration. In the QOGK an external source is used to drive a

prebunching resonator located upstream from the main resonator. Experiments have been carried out to investigate efficiency enhancement by mode priming and other regimes of operation, phase-locked operation, and operation as a linear amplifier. The efficiency of a conventional gyrotron or QOG is a sensitive function of a phase parameter which characterizes the detuning of the interacting mode. In a gyrotron with only one mode within the interaction bandwidth, the detuning can be optimized by adjusting the applied magnetic field or the electron gun voltage. The situation is more complicated if, as in the case of the QOG, there are several modes within the interaction bandwidth. Even if the final equilibrium state is single moded, there are several possible detunings with no guarantee that the one chosen by the system will be the most efficient. An important experimental result of the present work is that the oscillator start-up conditions can determine the efficiency of the equilibrium state. In a free-running, overmoded oscillator a sequence of successively lower frequency modes are excited as the relativistic cyclotron frequency decreases during the voltage rise. The term *mode priming* refers to a method of selecting one of several modes during the growth of RF fields in the main resonator. In the QOGK the drive signal, applied via the prebunching resonator, can stablize an efficient mode with respect to decay into competing modes allowing it to grow and ultimately nonlinearly supress neighboring modes. Efficiencies over 16% were obtained with this type of mode priming. Another method of varying the start-up conditions, called *alpha priming* was also investigated. In this mode of operation, the electron gun parameters are adjusted to increase the velocity pitch ratio ($\alpha = v_\perp/v_\parallel$) of the gyrating electron beam during the voltage rise in order to enhance the growth rate of the desired high-detuning mode. Operating this way led to the achievement of 19% electronic efficiency at 82 kW. By operating with a depressed collector the overall efficiency was increased to 30%.

Interest in the QOGK is also motivated by the need for phase and frequency stability in many applications. By applying the drive signal during steady-state oscillation, phase-locked operation could be investigated. In addition, by reducing the beam α to suppress self oscillation of the output cavity, the system could be operated as an amplifier.

There is currently considerable interest in compact, tunable radiation sources capable

of operating in the vibrational infrared (IR) (3—30μm)[12]. Conventional RF linac free-electron lasers (FELs) with magnetostatic wigglers can operate in this region, but their use is constrained by size, cost, and shielding requirements. The concept of an electromagnetic wiggler was introduced during the early work on FELs, and has been the subject of continuing interest as a means of reducing the required electron beam energy. However, there has been little experimental progress to date due to the lack of powerful wiggler radiation pump sources. The QOG is particularly well suited for use as a wiggler because of its ability to operate at short wavelengths with high efficiency, high circulating power, and long pulse lengths. Second harmonic QOGs can achieve wavelengths down to 600 μm, which represents a factor of $\sim$ 30 reduction in wavelength compared to conventional short-period magnetostatic wigglers. This enables the 3—5 μm IR atmospheric window to be reached using electron beam energies as low as 3 MeV, as compared to $>$ 20 MeV for RF linac FELs with conventional short-period wigglers. Electrostatic (ES) linear accelerators operating at a few MeV can be quite compact and their beam properties are well-matched to the QOG wiggler. Recirculation of the electron beam, a requirement for ES linac FELs, has the important benefit of greatly reducing the amount of x-ray shielding needed.

The remote sensing of upper atmosphere trace impurities is important to such vital environmental issues as ozone depletion, global warming, and climatic change. Ideally, one would like to conduct world-wide monitoring of mixing ratios of all important elements as functions of both altitude and time. Millimeter-wave radiametric measurements play an important role in this arena now. A difficulty with radiometry is that it takes a very long time, up to a week, to do these measurements due to the very low signal to noise level. An alternate scheme has been proposed by one of us[13] involving the use of a quasi-optical gyrotron with a large satellite tracking antenna. These satellite trackers are found all over the world and typically cost several million dollars each. Many of them have large antennas which are of sufficient quality that they can serve as high gain antennas for millimeter waves. The system would be tuned to a transition line of a trace impurity and would track a highly spherical satellite. The absorption and phase shift would then be measured as a function of frequency, and thereby the concentration of the impurity would be measured. This system

has several potential advantages compared to radiometry. First of all, the measurement time is dramatically reduced. Secondly, much more information is potentially available, because this measurement would give both absorption and phase measurements, as compared with radiometry, which has the capability of giving only absorption measurements. Thirdly, the system has the capability of giving spatial resolution along a line in the sky as it follows a particular satellite. Different satellite orbits would give resolution along different lines in the sky. Finally the system could be easily and quickly tuned from one frequency to another, so that different upper atmosphere impurities could be monitored fairly quickly. By using a system based on existing satellite trackers and perhaps ten target satellites, the measurements could be virtually worldwide and simultaneous.

The next section discusses our new experimental results. Section III discusses the design of IR FELs based on QOG powered electromagnetic wigglers, and Section IV discusses the sensing of upper atmosphere trace elements using an active system based on the QOG.

II Experimental Results

II-A Experimental Set-up

A schematic diagram of the quasioptical gyroklystron experiment is shown in Figure 2. The magnetic field is produced by a pair of modified Helmholtz coils in a cold-bore superconducting magnet with a crossbore. A magnetron injection gun (80 kV, 50 A) is mounted to a flange on the bottom of the magnet dewar and produces an annular electron beam in the fringing field of the coils. The pitch ratio of the beam electrons is controlled by varying the voltage applied to the intermediate anode of the electron gun via a resistive divider. The electron beam collector is located outside the magnet dewar and is electrically isolated from the rest of the experiment. This allows for depressed collector experiments by adding different resistances between the collector and ground. A trim coil is used so that nearly all of the beam current reaches the collector and is not intercepted by the uptaper.

The main resonator, located in the crossbore, comprises a pair of 5.5 cm-diameter mirrors with 38.7 cm radii of curvature. The resonator axis is tilted by $\sim 2°$ relative to the

plane perpendicular to the electron beam. Tilting the resonator axis allows each electron to interact with both even and odd longitudinal modes in the output resonator, which is predicted to increase the efficiency and region of stable, single-mode operation[14]. The output resonator mirror holders are mounted on precision micrometers so that the separation and alignment can be varied from outside the magnet dewar. A continuously tunable output resonator is particularly important in a gyroklystron experiment where the electrons should be bunched at the resonant frequency of the output resonator.

The drift tube is composed of alternating copper and ceramic rings to load spurious gyrotron oscillations in the high magnetic field region. A pair of capacitive probes are installed in the drift tube before and after the prebunching resonator which are used to determine the average α of the beam by measuring the longitudinal charge density. The drift tube is interrupted for 5 cm to allow for the prebunching resonator, which is formed by a pair of 3.1 cm diameter mirrors with radii of curvature 20 cm. The EIO signal is coupled into the prebuncher through a 1.8 mm diameter coupling hole in one of the mirrors. The opposite mirror also has a coupling hole which is used to monitor millimeter waves in the input resonator. The coupling aperture excites the TEM_{00} mode in the prebuncher with a total Q of 2000. A low-Q prebunching resonator is required to prevent oscillations in the input resonator, since strong oscillations will introduce a large energy spread on the beam and spoil the interaction in the output resonator. Input and detected signals are transmitted using standard WR-10 rectangular waveguide through vacuum windows mounted near the electron gun. The external source is a 1.5 kW, 85 GHz EIO with ± 1 GHz tuning and a variable pulse width up to 2 μsec. The voltage pulse produced by the gyrotron modulator has a 13 μsec flat top so that the external drive source is only used during a portion of the output pulse.

A summary of the parameters of the quasioptical gyroklystron experiment is given in Table 1. The maximum current of the experiment is limited by the threshhold current of the prebunching resonator, so that currents greater than 6 A are obtainable at the expense of lower α. The mirror separation is variable between 20–28 cm, although most of the data is collected for a separation of 21 cm. The radii of curvature of the mirrors is 38.7 cm,

Frequency	85.5 GHz
Beam Voltage	70 kV
Beam Current	6 A
Cavity Magnetic Field	33.42 kG
$\alpha = v_\perp/v_\parallel$	1.9
Mirror Separation	21 cm
Output Coupling	2%
Quality Factor	37 000
Interacting Modes	~4
Interaction Length μ	20

Table 1: Summary of the experimental parameters.

which results in a radiation waist of 1.39 cm near the center of the output resonator. The frequency separation between longitudinal modes in the output resonator is 0.83% for this mirror separation, which results in approximately 4 interacting modes.

II-B EIO Mode Priming

A new region of operation of the gyroklystron which has recently been demonstrated is mode priming. The output mirror separation is adjusted so that the two resonators have nearly the same frequency. Typical operating currents are 5 A so that the prebuncher does not oscillate, with a measured beam pitch ratio of $\alpha = 1.9$. The output rf pulse is displayed on the oscilloscope and the frequency is measured continuously using a heterodyne technique and bandpass filters. The gyrotron operates in a series of longitudinal modes with frequency separation $\Delta f = c/2L$ ~700 MHz, where L is the mirror separation. The output of the gyrotron is single-moded, and the frequency detuning and efficiency increase with increasing cathode voltage. As the voltage is increased past the maximum value for

a particular longitudinal mode, mode skipping occurs between the desired mode and a lower frequency, less-detuned mode. The output pulse skips from one mode to another on a pulse-to-pulse basis, determined by the noise present in the output resonator during the rise of the voltage pulse. A further increase in voltage results in 100% of the pulses occurring in the low frequency, low efficiency mode.

Figure 3 shows efficiency versus cathode voltage for EIO mode priming and free-running operation. The maximum efficiency obtained for the free-running oscillator for this case is 12% at a beam voltage of 66 kV. Above this voltage the output mode skips with the next lower-frequency longitudinal mode, causing the efficiency to drop. The EIO is used to prime the desired high-frequency mode near the cathode voltage where mode skipping begins. The EIO signal is injected on the rise of the voltage pulse to prebunch the electron beam. This bunched beam preferentially excites the 85.55 GHz mode, since the prebunching is much stronger than the noise present at the frequency of the competing mode. Now, 100% of the pulses occur in the desired mode, and the cathode voltage may be increased, which increases the detuning, to further increase the efficiency over the free-running oscillator value. The high-voltage limit of EIO mode priming is qualitatively different from the free-running oscillator. Here the desired 85.5 GHz mode is excited at the beginning of the pulse, but a lower frequency mode takes over during the remainder of the pulse and lowers the overall efficiency.

Mode priming the gyroklystron is only possible when the amplitude of the competing modes is small compared to the steady-state value. Once one of the modes grows in amplitude, mode priming becomes ineffective in determining the final state of the oscillator. As an example, consider the experimental conditions where the beam current is 5 A, the voltage divider is 82.5%, and the average pitch angle of the beam is 1.6. The maximum operating voltage for the 85.44 GHz mode is 71.6 kV, where the magnetic field at the center of the output resonator is 33.42 kG. The frequency detuning $(1 - \Omega/\gamma\omega)$ at this voltage is 3.63%, where the space charge depression across the output resonator is taken into account. If the EIO pulse is injected into the prebuncher after the voltage flat-top is reached, no mode priming is observed. Figure 4 shows the earliest the EIO can trigger and still prime

the 85.44 GHz mode in the output resonator. The EIO pulse occurs 1.4 μsec before the leading edge of the 13 μsec voltage pulse, which corresponds to a cathode voltage of 67 kV. Thus, the cathode voltage is 6% lower than its final value, with a corresponding frequency detuning of 2.9% at this point. Moving the EIO signal earlier in the voltage rise causes the mode priming to fail and the lower frequency mode is excited for 100% of the pulses.

II-C Alpha Priming

Another technique, denoted here as *alpha priming*, allows one to access large frequency detuning and high efficiencies by controlling the pitch angle of the electrons during the rise of the voltage pulse. This is accomplished by reducing the capacitance between the mod anode and the cathode via the resistive divider circuit. During free-running operation and EIO mode priming, α reaches its maximum value on the flat-top of the voltage pulse, whereas in alpha priming it occurs a slightly lower voltage. This excites a high frequency mode in the output resonator since $\omega \cong \Omega/\gamma$, where γ is the relativistic mass factor. This mode is highly detuned during the flat-top of the pulse and effectively suppresses competing modes. The limit for alpha priming is similar to that for EIO mode priming: competition from a low-frequency mode later in the pulse. This highly-detuned mode is obtained by varying the electron beam parameters on the rise of the voltage pulse and does not require any prebunching using the EIO.

A comparison of the three regimes of gyroklystron operation is shown in Figure 5, where efficiency is plotted as a function of beam current. Typical free-running oscillator efficiencies are on the order of 10%, while the EIO allows for mode priming up to 16% efficiency. Typical alpha-priming efficiencies are 19%, and demonstrate the benefit of increased voltage and detuning. The trend of falling efficiencies at higher currents is due to the reduction of the beam α so that the prebunching resonator does not oscillate.

The overall efficiency of the quasioptical gyroklystron can be further increased by depressing the collector. This is accomplished by adding different resistances between collector and ground. The performance of the gyroklystron is shown in Figure 6 as a function of

collector voltage depression. The gyrotron is operated in the alpha-primed regime with an electronic efficiency of 19% at a current of 6 A and 72 kV beam voltage. The maximum efficiency obtained is 30% for a collector depression of 35 kV, which corresponds to a collector efficiency of 50%. If the depression is increased further, electrons begin reflecting from the collector and rapidly degrade the oscillation in the main resonator. This work demonstrates that relatively high overall efficiencies can be obtained for high values of α and electronic efficiency.

II-D Phase-Locking and Amplifier Measurements

The term *phase locking* refers to the behavior of a nonlinear oscillator subjected to an external drive signal. If the drive source is sufficiently large in amplitude and close to the frequency of the free-running oscillator, the oscillator is pulled to the frequency of the drive. There is now a fixed phase relation between the input and output signals which depends upon the separation between the drive and free-running frequencies. For phase locking via direct injection into the output resonator, the fractional phase-locking bandwidth can be written

$$\frac{|f_d - f_0|}{f_0} = \frac{1}{Q_e}\sqrt{\frac{P_d}{P_0}}, \tag{1}$$

where Q_e is the external Q of the resonator and P_d and P_0 are the drive and output powers, respectfully. As the drive frequency is varied across the phase-locking bandwidth, the relative phase varies from $\frac{\pi}{2}$ to $\frac{-\pi}{2}$.

In the present experiment, phase locking is accomplished by prebunching the electron beam in an upsteam resonator using the EIO. Compared to direct injection, this technique requires less power to phase lock the oscillator due to the gain between resonators. The gyrotron is allowed to reach steady state, then the 2 μsec EIO pulse is turned on. Ideally, a continuous-wave source is preferred for the drive signal which could be frequency and phase locked using a phase-locked loop. Experimentally, the EIO is free running and has a measured pulse-to-pulse jitter of 3 MHz and a frequency chirp of 10 MHz during the 2

μsec pulse. This is to be compared to the 2.3 MHz FWHM of the high-Q output resonator in the gyroklystron. Thus, it is impossible to phase lock over the entire duration of the EIO pulse because of the chirp in the drive source and the narrow bandwidth of the output resonator.

As the EIO power to the prebunching resonator is decreased, the phase-locking bandwidth decreases. A plot of the measured phase-locking bandwidth versus input power is shown in Figure 7, along with the prediction of Adler's theory (Eq. 1). Although this equation is not applicable in the case of prebunching, Adler's relation is a benchmark for phase locking by direct injection. The experimental parameters are a beam voltage of 71.7 kV, a beam current of 5 A, and a magnetic field of 33.42 kG at the center of the output resonator. The voltage divider is 82.5%, with a measured value of pitch angle of 1.8. The output frequency of the gyrotron is 85.552 GHz and is single moded with an interaction efficiency of 16%. With no EIO attenuation, the gyroklystron is phase locked over the entire bandwidth of the output resonator at 25 dB below the output power level. The locking bandwidth decreases to ± 0.7 MHz when the drive signal is attenuated by 4 dB. These results are 20 dB below the drive power required for direct injection, and demonstrate the benefit of phase locking by prebunching the electron beam due to intercavity gain.

Two factors are important to achieving 100% reproducibility when phase locking the gyroklystron. First, the difference between the EIO and gyrotron frequencies should be minimum near the beginning of the 2 μsec EIO pulse. This reduces the amount of time required to lock the gyrotron to the EIO and improves pulse-to-pulse stability. Secondly, higher pitch angles allow for better phase locking due to the increased bunching parameter. Hence, the operating conditions for optimum power and efficiency coincide with those for optimum phase locking.

Although the gyroklystron is designed as an oscillator, it is possible to operate the device as an amplifier by lowering the average α of the beam so that the output resonator is below threshhold for oscillations. The output mirror separation is adjusted so that the output frequency matches the input resonator frequency. An oscilloscope trace of the output and input signals during amplifier operation is shown in Figure 8. The cathode voltage is 68.2

kV, the beam current is 6.5 A, and the voltage divider is 84.5%, resulting in a measured pitch angle of the electrons of 1.0. The output frequency is 85.556 GHz and is tuned to the resonance of the input resonator. No amplification is observed when the resonators are not matched in frequency.

The input pulse from the EIO is 2 μsec in duration, although the amplifier FWHM is only 0.6 μsec. This shortened pulse is due to the frequency chirp of the drive source coupled with the narrow resonance of the high-Q output resonator. The measured amplifier bandwidth is 2.4 MHz, which is in excellent agreement with the calculated output resonator bandwidth of 2.3 MHz and corresponding $Q = 37000$. In the past it has been speculated that the presence of the electron beam modifies the fields in the output resonator and causes higher diffraction losses and a lower quality factor. This work shows that the quality factor of the output resonator is not affected by the presence of the electron beam during amplifier operation.

Measured amplifier gain as a function of electron beam voltage is shown in Figure 9 for a beam current of 3.8 A. The voltage divider is 84.5% for this data. The gain increases monitonically from 6.5 to 17 dB as the voltage is increased during amplifier operation. The bandwidth of the gain is constant as a function of beam current and voltage, which indicates that the quality factor of the output resonator does not depend upon the beam in this regime. Cathode voltages above 67.5 kV cause the output resonator to oscillate. The efficiency of the amplifier at 67.5 kV is 9.5% and is not saturated for the present input source. The strong dependence of the gain on the cathode voltage is most likely related to two factors. First, the average α of the beam rises from 1.0 to 1.1 as the voltage is increased. Secondly, increasing the voltage increases the frequency detuning between the rf fields and the relativistic cyclotron frequency ($\Delta\omega = \omega - \Omega/\gamma$). Both of these effects increase the gain of the amplifier as the voltage is raised.

III QOG Wiggler FEL

The concept of an electromagnetic wiggler was introduced during the early work on FELs. The process of stimulated scattering with large energy exchange of a laser beam by

a relativistic electron beam was studied by Pantell[15]. The concept of a two-stage FEL in which the first stage provides the wiggler fields for the second stage and the same electron beam is used to drive both stages was presented by Sprangle and Smith[16], by Elias[17], and by Pasour *et al.*[18]. A microwave wiggler FEL was investigated experimentally by Granatstein et al.[19]. A visible wavelength FEL with a wave guided CO_2 laser pump was investigated by Gover, Tang and Sprangle[20]. The design of a soft x–ray FEL with a laser-powered wiggler was treated by Gea-Banacloche et al.[21], who also considered the design of a compact infrared FEL with a microwave wiggler[22]. The use of cavity-gyrotron-powered waveguide wigglers was considered by Danly et al.[23,24] and experimental results for a gyrotron-powered wiggler were obtained by Chu *et al.*[25].

This section discusses the design of IR FEL oscillators based on an electromagnetic wiggler powered by a quasioptical gyrotron. As in the configuration studied by Gea-Banacloche et al.[21], the wiggler fields are assumed to form a gaussian mode in an open mirror resonator. The system concept is illustrated in Fig. 10. In this figure the FEL and wiggler resonators are shown as coaxial with themselves and the electron beam. In practice, these axes may be slightly tilted with respect to each other, however, the coaxial assumption is used in the present analysis for simplicity. Pump field losses due to apertures in the wiggler resonator mirrors can be minimized by incorporating Bragg reflectors in the apertures[26]. The design constraints for optimum single-pass gain, an important FEL figure-of-merit, are obtained, including beam quality requirements.

III-A Cold Beam Gain Optimization

Consider a FEL in which the electron beam interacts with a counter-propagating electromagnetic "pump" wave contained in a quasioptical resonator. For a linearly polarized, lowest order gaussian mode in a Fabry-Perot resonator, the vector potential for the pump wave is given by:

$$A_x = \frac{E_0}{\omega}\frac{w_{p0}}{w_p(z)}\exp\left\{-i\left[\omega t + kz - \eta(z) + kr^2/2R(z)\right] - r^2/w_p^2\right\} \qquad (2)$$

where E_0 is the peak amplitude of the radiation electric field, ω is the angular frequency and k is the wavenumber of the pump radiation, w_{p0} is the radiation beam waist radius,

$w_p(z) = w_{p0}\sqrt{1 + z^2/z_p^2}$, $r^2 = x^2 + y^2$, $R(z) = z\left(1 + z_p^2/z^2\right)$, $\eta = \arctan z/z_p$, and z_p is the Rayleigh length. The resonance condition for a relativistic beam is:

$$\lambda_{IR} = \frac{\lambda_p}{4\gamma^2}\left(1 + a_w^2\right) \tag{3}$$

where λ_{IR} is the wavelength of the FEL radiation, λ_p is the wavelength of the pump radiation, γ is the relativistic mass factor, and a_w is the usual wiggler parameter. In the present regime a_w will be much less than unity so that it will be neglected in factors involving $1 + a_w^2$. Near the axis the amplitude of the vector potential is approximately given by:

$$|A_x| \approx \frac{E_{p0}}{\omega}\frac{w_{p0}}{w_p(z)}\left(1 - \frac{r^2}{w_p^2}\right) \tag{4}$$

As pointed out by Danly *et al.*[23], the wiggler field is slightly defocussing due to the $-$ sign in Eq.(4). However, this is a weak effect when $a_w^2 \ll 1$, as is usually the case, and could be compensated by external focusing if necessary. The peak small-signal gain per pass for a FEL with a cold filamentary electron beam in the low-gain Compton regime can be expressed in the form[21]:

$$G^{(c)} = -4\pi^2\frac{\lambda_{IR}^{3/2}\lambda_p^{1/2}}{\sigma_{IR}}\left\langle a_w^2\right\rangle N^3\frac{I}{I_A}0.54 \tag{5}$$

where σ_{IR} is the FEL mode area, I is the electron current within the mode area, $I_A = 4\pi mc^2/(Z_0 e) \sim 17000$ A is the Alfven current, N is the number of wiggler periods, $\langle a_w^2\rangle$ denotes an average over the interaction length, and $Z_0 = 377$ ohms. Assuming the interaction length corresponds to two Rayleigh lengths, the average wiggler parameter is related to the pump maser circulating power (P_m) according to:

$$\left\langle a_w^2\right\rangle = \frac{\lambda_p^2 P_m}{16\pi w_p^2 P_0} \tag{6}$$

where $P_0 = \pi m^2 c^4/(2e^2 Z_0) = 1.09$ GW. The effective interaction length L_{int} in a quasioptical resonator is taken to be twice the Rayleigh length. The resonator mirror separation is assumed to be at least $2z_p$. The electron beam and the pump wave pass through each other at essentially the same speed so that the number of wave periods encountered by an

electron passing through the wiggler is given by:

$$N = \frac{4z_p}{\lambda_p} = 4\pi \left(\frac{w_p}{\lambda_p}\right)^2 . \tag{7}$$

The minimum radiation waist of the wiggler mode is determined by the number of wiggler periods according to Eq.(7). Similarly, to avoid coupling losses due to diffraction of the FEL radiation, the Rayleigh length of the FEL mode should be at least as long as the wiggler mode Rayleigh length. For the case of equality, this fixes the minimum radiation waist of the FEL mode as:

$$w_{IR} = w_p \sqrt{\frac{\lambda_{IR}}{\lambda_p}}, \tag{8}$$

The FEL radiation beam waist constrains the maximum size of the electron beam radius consistent with low coupling losses. For the case of the lowest order gaussian mode, the effective FEL mode area is given by: $\sigma_{IR} = \pi w_{IR}^2/2$[27]. Thus, to match the electron beam cross section to the effective area of the radiation beam requires: $r_b \leq w_{IR}/\sqrt{2}$.

Using these relationships, substituting for a_w, leads to the following expression for the peak cold beam gain using an electromagnetic wiggler:

$$G_{em}^{(c)} = 8\pi^2 \sqrt{\frac{\lambda_{IR}}{\lambda_p}} \frac{P_m}{P_0} \frac{I}{I_A} N\,(0.54) \tag{9}$$

III-B FEL Electron Beam Quality Requirements

The achievable electron beam quality places significant restrictions on the parameters of the FEL available for operation near the cold-beam limit. The homogeneous gain bandwidth corresponds to the range $\theta = 0$ to $\theta = \pi$, where $\theta = 2\pi N\,(\delta\gamma/\gamma)$ characterizes the detuning of the electron energy from resonance. To operate near the cold beam regime, the inhomogeneous broadening associated with beam energy spread, emittance, transverse wiggler gradients, and space charge should be less than the homogeneous gain bandwith. Gover and Jerby have shown that, to a good approximation, the effect of finite beam quality can be taken into account by modifying the gain expression as follows[28]:

$$G_{em}\,(\theta_{th}) = \frac{G_{em}^{(c)}}{(1 + \theta_{th}^2/\pi^2)} \tag{10}$$

where $\theta_{\rm th}$ is a detuning spread parameter associated with inhomogeneous broadening effects such as beam energy spread and transverse wiggler field inhomogeneities. The detuning spread due to energy spread is given by[28]:

$$\theta_{\rm th,1} = 2\pi N \frac{\Delta E}{E} \tag{11}$$

The detuning due to finite emittance is given by[28]:

$$\theta_{\rm th,2} = 2\pi N \frac{\epsilon_{\rm n}^2}{r_{\rm b}^2} \tag{12}$$

where $\epsilon_{\rm n}$ is the normalized emittance. The detuning spread due to space charge is given by[28]:

$$\theta_{\rm th,3} = 2\pi N \frac{\nu}{\gamma} \tag{13}$$

where Budker's parameter is given by: $\nu = \gamma I / I_{\rm A}$. The detuning due to the transverse field inhomogeneity in a gaussian wiggler is given by a straight forward extension of the result for a waveguide mode wiggler given in Ref. [23]:

$$\theta_{\rm th,4} = 4\pi N a_{\rm w}^2 r_{\rm b}^2 / w_{\rm p}^2 \tag{14}$$

The total detuning is given by:

$$\theta_{\rm th} = \sqrt{\sum_{\rm i=1}^{4} \theta_{\rm th,i}^2} \tag{15}$$

To avoid a large reduction in the gain from the cold beam value, each of the above detuning parameters should be less than π radians. The detuning effect due to transverse wiggler gradients is typically very small for millimeter-wave electromagnetic wigglers. Expressing the FEL mode area and pump mode radiation waist in terms of the number of wiggler periods, and accounting for energy spread, finite emittance, space charge, and wiggler transverse gradient detuning effects, leads to the following expression for the warm-beam electromagnetic wiggler FEL gain:

$$G_{\rm em}^{(\rm w)} = 8\pi^2 \sqrt{\frac{\lambda_{IR}}{\lambda_{\rm p}} \frac{P_{\rm m}}{P_0} \frac{I}{I_A}} N\,(0.54) \cdot \left[1 + \left(2N \frac{\Delta E}{E} \right)^2 + \left(\frac{16\pi\epsilon_{\rm n}^2}{\lambda_{\rm p}\lambda_{\rm IR}} \right)^2 + \left(\frac{2NI}{I_A} \right)^2 + \left(\frac{N a_{\rm w}^2}{\gamma^2} \right)^2 \right]^{-1} \tag{16}$$

III-C QOG Wiggler

The quasioptical gyrotron has generated high power at high efficiency. The highest output power is about 600 kW at 2.2 mm wavelength[9]. If the quasioptical gyrotron is to be used as a wiggler for an FEL, the figure-of-merit is not the output power, but the circulating power. Since the output at high power was about 3% per pass, the circulating power was about 20 MW. Thus the power has to be increased by a factor of five or more and the wavelength must be decreased by a factor of two to produce a wiggler sufficient to generate 6μm radiation with a 3 MeV electron beam. The required increase in circulating power and decrease in operating wavelength can both be obtained from working at the second harmonic of the cyclotron frequency. Efficient operation at the harmonic is theoretically possible, provided that the fundamental harmonic can be supressed, but the optimum fields are higher than for fundamental operation. However, this is advantageous, since higher fields correspond to higher circulating power.

The use of normalized variables to express the equations of motion in terms of a small number of parameters has proven extremely useful for gyrotron design optimization. The slow-time-scale (STS) (averaged with respect to the cyclotron period) equations for the interaction with a single resonator mode can be characterized by the harmonic number s, the normalized electric field amplitude (F_s), interaction length (μ), and detuning parameter Δ. These parameters are given in terms of the unnormalized parameters expressed in MKS units (which are used throughout) as follows:

$$F_s = \frac{e}{2\pi mc^2}\frac{s^s}{2^{s-1}s}\frac{1}{\gamma_m \beta_{\perp m}^{4-s}} E_m \lambda_p \tag{17}$$

$$\mu = \frac{2\pi\beta_{\perp m}^2}{\beta_{\|m}}\frac{w_m}{\lambda_p} \tag{18}$$

$$\Delta = \frac{2}{\beta_{\perp m}^2}\left(1 - \frac{seB_0\lambda_p}{2\pi mc\gamma_m}\right), \tag{19}$$

where E_m is the peak amplitude of the counter-propagating wave in the maser, s is the harmonic number of the electron cyclotron maser interaction, γ_m is the relativistic factor for the maser electron beam, and $\beta_{\|m}$ and $\beta_{\perp m}$ are the parallel and perpendicular velocities of the gyrating maser beam normalized to c. Note that the RHS of Eq.(17) would contain an

additional factor of two if F_s were expressed in terms of the peak standing wave amplitude. The electronic efficiency can be written in the form: $\eta = \eta_{sp}\hat{\eta}$ where η_{sp} is the is the single particle efficiency given by:

$$\eta_{sp} = \frac{\beta_{\perp m}^2}{2\left(1 - \gamma_m^{-1}\right)} \tag{20}$$

and $\hat{\eta} = \hat{\eta}(F_s, \mu, \Delta, s)$ is the normalized efficiency obtained by solving the STS equations of motion. For a given harmonic, and optimized detuning, $\hat{\eta}$ depends only on F_s and μ, and the results can be presented as an $F - \mu$ plot of the iso-efficiency contours. Results for $s = 2$ are shown in Figure 11. The efficiency results shown in these figures are directly applicable only in the low mode density regime wherein the achievable detuning is not limited by mode competition. However, as shown by Antonsen *et al.*[14] and the experimental results presented herein, high mode density does not preclude efficient single-mode operation. The QOG circulating power may be expressed in terms of the normalized parameters as follows:

$$P_m = \frac{\pi m^2 c^4}{8e^2 Z_0}\left(\frac{2^{s-1}s!}{s^s}\right)^2 \gamma_m^2 \beta_{\|m}^2 \beta_{\perp m}^{4-2s} \left(F_s \mu\right)^2 . \tag{21}$$

The QOG electron beam power required to sustain a given circulating power depends on the resonator losses and the interaction efficiency. The interaction efficiency can be estimated using an $F - \mu$ plot as discussed above. The losses include the ohmic power dissipated on the mirrors and diffractive losses. The power lost to FEL interaction is negligible. The total ohmic power lost on a smooth mirror in a Fabry-Perot resonator scales with the maser circulating power according to:

$$P_{ohm} = 2\left(\frac{\pi}{Z_0 \sigma \lambda_p}\right)^{1/2} P_m \tag{22}$$

where σ is the conductivity. For copper at 200° C, $\sigma = 3.6 \times 10^7$ siemens/m. This leads to an ohmic loss per mirror of about 0.1% P_m for $\lambda_p \sim 1$ mm. These losses may be several times larger if the mirror surface includes a diffraction grating for frequency selectivity.

III-D Frequency Selective Resonator

The simplest high-Q resonator for the QOG consists of a pair of spherical mirrors. The mirror diameter can be chosen to provide a specific amount of output coupling via diffraction

around the mirror edge, as well as high diffraction losses for higher order transverse modes of the resonator. The mirror edge diffraction loss decreases with increase in frequency, which leads to some selectivity for the higher harmonic interactions. Stronger frequency selectivity may be obtained by replacing one of the mirrors by a diffraction grating placed in the Littrow-mount condition as shown in Fig. 12. If the groove spacing (d) satisfies the condition:

$$d = \frac{\lambda}{2\sin\theta} \tag{23}$$

where θ is the angle of incidence, then the $n = -1$ diffraction order of the grating is reflected back into the resonator and the 0 order, which is specularly reflected, is coupled out. If $\lambda/d < 2/3$, then only the 0 and -1 order waves are diffracted. The depth of the grooves (h) determines the efficiency of the -1 grating order and can be chosen such that efficiency of the -1 order is 100% for the TM polarization and an ideal grating[29]. This effect can be obtained with "blazed," sinusoidal, and rectangular groove shapes. For example, the $n = -1$ efficiency of an ideal rectangular groove grating is 100% for the TM polarization when $h/d = 0.2$ and $\lambda/d \sim 1.5$[29]. The design of a grating for the maser resonator must account for the curved surface of the gaussian mode wavefront. This leads to the need to use curved grooves with nonuniform spacing in order to satisfy the Littrow condition at all points on the grating[30]. With careful design diffraction losses associated with these effects should be limited to a few tenths of a percent. If the resonator is designed for fundamental harmonic operation, the Littrow condition can only be satisfied for higher harmonic radiation at a higher diffraction order, which will usually have lower efficiency than than the -1 order of the fundamental harmonic radiation. If the resonator is designed for operation in a higher harmonic, the Littrow condition will not be satisfied for the lower harmonics which will be coupled out of the resonator by specular reflection. Thus the Littrow-mount grating should be very effective at discriminating against lower-order harmonic interactions. Theory and experimental data indicate that ohmic losses are several times higher for a grating than a smooth surface[31]. Littrow-mount diffraction gratings have also been investigated as output couplers for quasioptical gyrotrons. In this application, the grating must not only return the -1 order efficiently to the resonator,

it must also provide focusing for the output beam. Recent cold-test measurements have demonstrated that high quality gaussian mode output beams can be obtained[32,33].

III-E Point Design

Design parameters have been obtained for a tunable IR FEL oscillator with operating range of 6—12 μm. The recirculating electron beam is generated by an electrostatic (ES) linac, and the pump field is provided by a second harmonic QOG operating at 1200 μm. The required beam energy for 6 μm radiation is 3.1 MeV. Tuning to longer wavelengths is achieved by reducing the FEL beam energy (to 2.1 MeV for 12 μm). The wiggler parameters are held constant during frequency tuning. The peak output power at 6 μm is 10 kW. The power decreases at longer wavelengths due to the reduction in beam voltage: i.e., at 12 μm the peak power is 7 kW.

The parameters of the QOG wiggler–ES linac FEL are given in Table 2. The approximate size of the ES linac would be: 16 ft. long, 4 ft. diameter, and 5,000 lb. weight. The FEL electron beam parameters have been chosen to be consistent either with values achieved by the UCSB FEL, or with design values of ES linac FELs under development at CREOL[34] and UCSB[35]. The quasioptical gyrotronparameters are listed in Table 3. The specified pump maser parameters include the output (pump) wavelength (λ_p), the harmonic number of the maser interaction (s), the maser beam gyration pitch angle (α), the maser voltage, and the product of the normalized parameters F, μ.

The design is based on a 750 period wiggler with an effective length of 45 cm. The wiggler circulating power is 140 MW and the average wiggler parameter is $a_w = 0.005$. The small signal warm beam gain is 4.9% for 6 μm radiation and increases at longer wavelengths. The main sources of resonance thermalization are the emittance and space-charge. There is very little detuning spread due to wiggler gradients or for beam energy spread for an ES linac.

Beam Energy	3.1 MeV
Beam Current	5.0 A
Normalized Emittance	10 π mm mrad
Relative Energy Spread	0.014%
Beam Diameter	0.9 mm
Beam Current Density	740 A/cm^2
Wiggler Wavelength	1200 μm
Number of Wiggler Periods	750
Interaction Length	45 cm
Wiggler Radiation Waist Diameter	18.6 mm
Wiggler Power Density	104 MW/cm^2
Maximum a_w	0.0074
FEL IR Radiation Waist Diameter	1.3 mm
Efficiency	0.07%
Output Power	10.4 kW
Warm Beam Gain per Pass	4.9%

Table 2: 6 μm FEL design parameters.

Frequency	250 GHz
Harmonic Number	2
Voltage	150 kV
Current	68 A
Magnetic Field	57 kG
$\alpha = v_\perp / v_\parallel$	1.25
Resonator Losses	1%
Peak Circulating Power	140 MW
Peak Output Power	1.4 MW
Electronic Efficency	14%
Collector Efficiency	50%
Overall Efficiency	24%

Table 3: Parameters of QOG wiggler for 6 μm FEL.

IV Remote Sensing of Upper Atmospheric Impurities

IV-A Formulation of the Problem

A schematic of the active sensor system is shown in Fig. 13. We envision that a pulse from the QOG is fed into the antenna of a large, millimeter-wave capable satellite tracker. If the QOG is operated as a free-running oscillator, the output waveform will vary slightly from pulse to pulse. It will be necessary to record exactly what the transmitted waveform is, and also to associate a particular received waveform with its transmitted counterpart. This can be done in the following way. Say that the transmitted waveform is given by

$$E_t(t) = \int G_t(f) \exp(2\pi i f t) df \equiv e_t(t) \cos[2\pi f_0 t + \phi_t(t)] \tag{24}$$

Here f_0 is assumed to be the carrier frequency and ϵ and ϕ are assumed to vary very slowly in time compared with f_0. We adopt a notation using E as a dependent variable in the

time domain and G as a dependent variable in the frequency domain. We assume then that e and ϕ can be digitized and computer analyzed. The digitizing does not have to be nearly fast enough to resolve f_0. By mixing the transmitted signal with a pair of local oscillator signals, one proportional to $\cos(2\pi f_0 t)$ and the other proportional to $\sin(2\pi f_0 t)$, and sending the two mixed signals through a low-pass filter, we can determine $\epsilon_t(t)$ and $\phi_t(t)$. We will discuss the requirements on the A:D convertors shortly.

When the signal propagates through the atmosphere, each frequency component has a different attenuation and phase shift depending on the impurity and its concentration. Therefore, from e and ϕ, the first task is to obtain G, the Fourier transform of the signal, defined by

$$G_t(f) = \int e_t(t) \cos[2\pi f_0 t + \phi(t)] \, exp(-2\pi i f t) dt. \tag{25}$$

Assuming that the fastest variation is from f_0 and that we are looking at $f > 0$ (the assumption is always that $f_0 > 0$), we find that

$$G_t(f) \cong \frac{1}{2} \int e_t(t) \exp\{i[2\pi \delta f t + \phi(t)]\} dt \tag{26}$$

where $\delta f = f_0 - f$. Thus the Fourier transform can be calculated from only a knowledge of e and f on a time-scale much slower than that required to resolve f_0, that is, a time-scale on which the data can be digitized.

There will also be a received signal, and the amplitudes, phases and Fourier transform can be determined in the same way. Now consider how to solve for the atmospheric attenuation and phase shift. The received frequency will be denoted by f. Since the satellite has a known velocity v toward the tracker, the transmitted frequency which will be received at f if it is transmitted at $f - 2vf_0/c$, where f_0 is the center frequency and we neglect effects of order $\delta f v/c$. Thus the transmitted spectrum corresponds to the transform $G_t(f - 2vf_0/c)$. This is absorbed and phase shifted on the way up by an amount $A(f - 2vf_0/c)$, where A is a complex function of frequency. Then the incident wave is reflected from the satellite. Since the satellite is assumed to be perfectly spherical, the reflection is independent of the satellite orientation and rotation. The complex reflection coefficient is therefore a known function of frequency and is denoted $R(f - vf_0/c)$. The radiation is absorbed in the atmo-

sphere by an amount $A(f)$ during the return path. Now G_t, G_r, and R are all known, so that

$$A(f - 2vf_0/c)\,A(f) = \frac{G_r(f)}{G_t(f - 2vf_0/c)\,R(f - vf_0/c)} = Q(f) \tag{27}$$

The right hand side is a known function of f, although it is only known to within arbitrary phase and amplitude factors unless the range to the satellite is known to within a fraction of a wavelength. However, the quantities of interest are the variations of the absorption and phase shift as a function of frequency, and Eq.(27) does give this.

Eq.(27) is complicated by the fact that it is not an equation for A itself, but the equation for a product of the A's at two different frequencies. For a low earth orbit satellite, and an absorber at 40 km, the frequency shift $2vf_0/c$ is smaller than, but comparable to, the width of the line. The optimum solution for A must be determined in each particular case. For the case of $2vf_o/c$ small or comparable to the width of the line, a power series expansion could be a reasonable approximation. If we take

$$A(f - 2vf_0/c) = \sum_n A_n(f)\,(2vf_0/c)^n \tag{28}$$

then the first three terms in the expansion are

$$A_0 = \sqrt{Q},\ A_1 = A_0'/2,\ A_2 = A_0'^2/8A_0. \tag{29}$$

where the prime denotes the deriviative with respect to f.

IV-B System Requirements

We first consider the requirements on the data processing, and specifically those on the A:D converter necessary to digitize the data. A useful approximation is a time and band limited function, even though strictly speaking, such a function cannot be physically realized. The Gaussian waveform with the linear chirp is a reasonable approximation to a time-limited, band-limited function, and other functions may be better still. The transmitted pulse is assumed to be limited to time between 0 and T_t. The received pulse is then limited to times between $2R/c$ and $T_t + 2R/c$, where R is the range.

Since the incident and returned signals are limited in time to a time we call T_0, we can regard these signals as periodic with period T_0 as long as we are careful to always

stay within the time $0 < t < T_0$. Thus the signal can be regarded as a discrete Fourier summation of the form

$$e(t) = \sum_n g_n e^{i2\pi nt/T_0} \tag{30}$$

If the signal is band-limited as well as time-limited, then g_n is non-zero only for $|n| < N$. Then $e(t)$ is needed only at $2N$ discrete, equally spaced values of t to solve for the $2N$ values of g_n. Thus the envelop waveforms $e(t)$and $\phi(t)$ must be sampled twice per period at the maximum frequency, and this gives all the information there is to be had about the function. Since the bandwidths we are interested in are tens of megahertz, a 100 MHz A:D converter, which is much less than the maximum available capability, would be more than adequate to digitize the data.

We now consider the requirements on the satellite. Let us say that it is spherical with an error in radius δr. If δr were zero, the reflection from the satellite would be perfectly calibrated as a function of frequency. However, because it is not zero, the reflection has slight phase and amplitude errors. For instance, if we interpret the δr as a random position of a scattering center, and consider a spectrum of width δf, then the relative phase error, compared to the phase of the central frequency is about $4\pi\delta r\delta f/c$. If we consider a line width of about 10 MHz, characteristic of 40 km altitude, the phase error as one crosses the line is about $4 \times 10^{-3}\delta r$(cm). For a weak absorber with a Lorentzian line shape, the phase shift across the line is roughly the attenuation. There is experience both in manufacturing highly spherical balls and in launching them into space. For instance, the Salem Specialty Ball Corporation in West Simsbury, Connecticut manufactures a chromium steel ball, 15 cm in diameter, and weighing about 30 pounds, with a surface tolerance of about 5 μm. Submicron tolerances are possible, as are hollow balls as large as 30 cm in diameter with comparable surface finish[36]. However, even with current manufacturing tolerance, phase accuracies of 2×10^{-6} radians are possible.

There is currently a NASA project which is launching six of these balls into space. It is called the *Orbital Debris Radar Callibrated Sphere Project* and it will be launched on the Shuttle STS 53 scheduled for launch on December 2, 1992. In March, 1993, another shuttle with additional balls is being launched. The purpose of the NASA project is to callibrate

the orbits and radar cross sections of space debris. Unfortunately, the balls will be orbited at an altitude of only ~ 170 nautical miles, so the lifetime of the balls in orbit will only be about 5 months. However, it would not be difficult to launch another series of balls into an orbit with an altitute of greater than 200 miles, for which the lifetime would be many years. On a future shuttle flight, 6 inch diameter balls could be launched into such an orbit for less than a million dollars[37].

The phase accuracy of the measurement is also limited by noise. The accuracy of a phase measurement (in radians) goes roughly as $1/\sqrt{S}$, where S is the signal-to-noise ratio. With the proposed system, this can be reduced somewhat by integrating over several different pulses. However, one does not have the same flexibility as in a radiometry measurement, because the measurement must occur while the satellite is passing overhead. Thus, to resolve weak absorbers, a cooled receiver could be used to reduce the noise level. We consider a receiver temperature of 20°K.

IV-C Examples for Ozone and Chlorine Monoxide

Ozone is a fairly strong absorber. Its opacity at 110.8 GHz is about 0.2 for two-way propagation at an angle of 45°, so the phase shift across the absorption line is about 0.2 radians. Let us consider the quasioptical gyrotron at this frequency with a power of 1 MW. If the range is 40 km, the receiver bandwidth is the transmitted line width, 10 MHz, the satellite is a sphere with radius 7.5 cm, and the antenna is a 20 m diameter satellite tracker, we find the signal-to-noise ratio is about 10^6. Thus, we can easily resolve the absorption line for ozone, or any correspondingly strong absorber. In fact, to resolve the ozone, one needs neither a cooled receiver nor the full power of the QOG.

Now consider ClO. This is a much weaker absorber: according to Parrish, the opacity is about 3×10^{-4} for two-way propagation at 45°[38]. This is the accuracy at which the phase and amplitude must must be measured. The satellite has sufficient accuracy for the measurement. However, the signal-to-noise ratio must be about 10^8 or greater. We consider the 242 GHz absorption line of ClO. At this frequency, the received signal is reduced by atmospheric attenuation. For a relative humidity of 50% and a zenith angle of 45°, the

two-way attenuation is about 10 dB. This could be substantially reduced by locating the tracker on a mountain top. For a transmitted power of 1 MW and the system otherwise the same as for ozone detection, $S \sim 5 \times 10^5$. Thus, about 200 pulses would be needed to bring the signal-to-noise level up to that required. For 10 μs pulses at 100 Hz, this measurement would take about 2 seconds, a short enough time that the satellite will not move very far in the sky.

V Acknowledgments

The authors gratefully acknowledge helpful discussions with P. Sprangle, S. Gold, B. Levush, T. Antonsen,Jr., M. Q. Tran and M. Sundquist. This work was supported by the Office of Naval Research.

References

[1] P. Sprangle, J. Vomvoridis, and W.M. Manheimer, "A classical electron cyclotron quasioptical maser," *Appl. Phys. Lett.* **38**, 310 (1981); and "Theory of the quasioptical electron cyclotron maser," *Phys. Rev. A* **23**, 3127 (1981).

[2] T.A. Hargreaves, K.J. Kim, J.H. McAdoo, S.Y. Park, R.D. Seeley, and M.E. Read, "Experimental Study of a Single-Mode Quasi-Optical Gyrotron," *Intl. J. Electronics*, **57**, 977 (1984).

[3] M.E. Read, M.Q. Tran, J. McAdoo, and M. Barsanti, "Experimental Study of a 115 GHz Quasi-Optical Gyrotron," *Intl. J. Electronics* **65**, 309 (1988).

[4] A.W. Fliflet, T.A. Hargreaves, W.M. Manheimer, R.P. Fischer, and M.L. Barsanti, "Operation of a Quasi-Optical Gyrotron with Variable Mirror Separation," *Phys. Rev. Lett.* **62**, 2664 (1989).

[5] A.W. Fliflet, T.A. Hargreaves, W.M. Manheimer, R.P. Fischer, M.L. Barsanti, B. Levush, and T. Antonsen,Jr., "Operating Characteristics of a Continuous-Wave Rele-

vant Quasi-Optical Gyrotron with Variable Mirror Separation," *Phys. Fluids B* **2**, 1046 (1990).

[6] A.W. Fliflet, T.A. Hargreaves, W.M. Manheimer, R.P. Fischer, and M.L. Barsanti, "Initial Operation of a high power quasi-optical gyrotron," *IEEE Trans. Plasma Science* **18**, 306 (1990).

[7] A.W. Fliflet, T.A. Hargreaves, R.P. Fischer, W.M. Manheimer, and P. Sprangle, "Review of Quasi-Optical Gyrotron Development," *Fusion Energy* **9**, 31 (1990).

[8] T.A. Hargreaves, A.W. Fliflet, R.P. Fischer, and M.L. Barsanti, "Depressed collector experiments on a quasioptical gyrotron," *Phys. Fluids B* **3**, 3171 (1991).

[9] T.A. Hargreaves, A.W. Fliflet, R.P. Fischer, M.L. Barsanti, W.M. Manheimer, B. Levush, and T. Antonsen, Jr., "Tilted resonator experiments on a quasioptical gyrotron," *Int. J. Electronics*, **72**, 807 (1992).

[10] S. Alberti, M.Q. Tran, J.P. Hogge, T.M. Tran, A. Bondeson, P. Muggli, A. Perenoud, B. Jödicke, and H.G. Mathews, "Experimental measurements on a 100 GHz frequency tunable quasioptical gyrotron," *Phys. Fluids* **2**, 1654 (1990).

[11] J. P. Hogge, M. Pedozzi, M.Q. Tran, T. M. Tran, H. Cao, and P. J. Paris, "Operation of a quasi-optical gyrotron with a gaussian output coopler," Conference Digest, The 17th International Conference on Infrared and Millimeter Waves, Pasadena, CA, December 14–18, 1992.

[12] D. D. Dlott and M. D. Fayer, "Applications of infrared free-electron lasers: basic research on the dynamincs of molecular systems," *IEEE J. Quant. Elect.* **27**, 2697 (1991).

[13] W. M. Manheimer, "On the possibility of high power gyrotrons for super range resolution radar and atmospheric sensing," *Int. J. Elect.* **72**, 1165 (1992).

[14] T.M. Antonsen, Jr., Jr, B. Levush, and W.M. Manheimer, "Stable single mode operation of a quasioptical gyrotron," *Phys. Fluids B*, vol. 2, no. 2, p. 419, 1990.

[15] R. H. Pantell, G. Soncini, and H. E. Puthoff, "Stimulated Photon–Electron Scattering," *IEEE J. Quant. Electron.***QE-4**, 905 (1968).

[16] P. Sprangle and T. Smith, "Theory of free-electron lasers," *Phys. Rev. A***21**, 293 (1980).

[17] L. R. Elias, "High-power, cw, efficient tunable (uv through ir) free-electron laser using low-energy electron beams," *Phys. Rev.Lett.***42**, 977 (1979).

[18] J.A. Pasour, P. Sprangle, C.M. Tang, and C.A. Kapetanakos, "High-power, Two-Stage FEL Oscillator Operating in the Trapped Particle Mode," *Nucl. Instr. and Meth. in Phys. Res.***A237**, 154 (1985).

[19] V. L. Granatstein, Y. Carmel, and A. Gover,"Demonstration of a free electron laser with an electromagnetic wiggler," in *Free-Electron Generators of Coherent Radiation* SPIE Proceedings Volume 453, 344 (1983).

[20] A. Gover, C.M. Tang, and P. Sprangle, "Feasibility of D.C. to Visible High Power Conversion Employing a Stimulated Compton free-electron Laser with a Guided Wave CO_2 Laser Pump Wave and an axial Electric Field," *J. Appl. Phys.* **53**, 124 (1982).

[21] J. Gea-Banacloche, G. T. Moore, R. R. Schlicher, M. O. Scully, and H. Walther, "Soft x-ray free-electron laser with a laser undulator," *IEEE J. Quant. Electronics* **QE-23**, 1558 (1987).

[22] J. Gea-Banacloche, G. T. Moore, R. R. Schlicher, M. O. Scully, and H. Walther, "Proposal for a compact FEL with electromagnetic-wave undulator," *Nucl. Instr. and Meth. Phys. Res.* **272**, 199 (1988).

[23] B. G. Danly, G. Bekefi, R. C. Davidson, R. J. Temkin, T. M. Tran, and J. S. Wurtele, "Principles of gyrotron powered electromagnetic wigglers for free-electron lasers," *IEEE J. Quant. Electronics* **QE-23**, 103 (1987).

[24] T. M. Tran, B. G. Danly, and J. S. Wurtele, "Free-electron lasers with electromagnetic standing wave wigglers," *IEEE J. Quant. Electronics* **QE-23**, 1578 (1987).

[25] T.S. Chu, B.G. Danly and R. Temkin, "A gyrotron-powered standing-wave electromagnetic wiggler experiment," *Nucl. Instr. and Meth. in Phys. Res.* **285**, 246 (1989).

[26] P. Sprangle, B. Hafizi, and F. Mako, "New x-ray source for lithography," *Appl. Phys. Lett.* **55**, 2559-2560 (1989).

[27] A. Gover, H. Freund, V. L. Granatstein, J. H. McAdoo, "Basic design considerations for FELs driven by electron beams from RF accelerators," *Infrared and Millimeter Waves*, vol. 11, Ch. 8, K. J. Button, Ed. (New York:Academic), (1984).

[28] E. Jerby and A. Gover, "Investigation of the gain regimes and gain parameters of the free-electron laser dispersion equation," *IEEE J. Quant. Electronics* **QE-21**, 1041 (1985).

[29] D. Maystre, M. Neviere, and R. Petit, "Experimental Verifications and Applications of the Theory," *Electromagnetic Theory of Gratings*, R. Petit,Ed., Springer-Verlag, (New York, 1980), Chap. 6.

[30] J.P. Hogge, H. Cao, W. Kasparek, and T.M. Tran, "Output coupling of a quasi-optical Fabry-Perot resonator by means of a diffractive grating in the mm-wave range," Conference Digest of the Fifteenth Int. Conf. on Infrared and Millimeter Waves, 10-14 Dec. 1990, Orlando, FL, R.J. Temkin, ed., SPIE **1514**, 535.

[31] R.P. Leavitt, D.E. Wortman, and H. Dropkin, "Millimeter-wave Orotron Oscillation–Part I: Theory," *IEEE J. Quantum Electronics* **QE-17**, 1333 (1981).

[32] H. Cao, J.P. Hogge, T.M. Tran, and M.Q. Tran, "Distortion and cross polarization of a simple gaussian beam on diffraction from grating couplers for Q.O. gyrotrons," Conference Digest of the Sixteenth Int. Conf. on Infrared and Millimeter Waves, 26-30 August 1991, Lausanne, Switzerland, R.J. Temkin, ed., SPIE **1576**, 542.

[33] J.P. Hogge, H. Cao, W. Kasparek, T.M. Tran, and M.Q. Tran, and P.J. Paris, "Ellipsoidal Diffraction grating as output coupler for quasi-optical gyrotrons," Conference

Digest of the Sixteenth Int. Conf. on Infrared and Millimeter Waves, 26-30 August 1991, Lausanne, Switzerland, R.J. Temkin, ed., SPIE **1576**, 540.

[34] L.R. Elias I. Kimel, D. Larson, D. Anderson, M. Tecimer, and Z. Zhefu, "A compact cw free-electron laser," *Nucl. Instr. and Meth. in Phys. Res.* **A304**, 219 (1991).

[35] G. Ramian, "Properties of the new UCSB free-electron lasers," *Short-Wavelength Radiation Sources*, Phillip Sprangle, Editor, Proc. SPIE 1552, 69 (1991).

[36] R. Presutti, private communication, November 1992).

[37] J. Stanley, private communication, LBL Space Flight Center Houston TX, Nov 1992).

[38] A. Parrish, R. DeZafra, P. Soloman, J. Barrett, *Radio Science* **23**, 106 (1988).

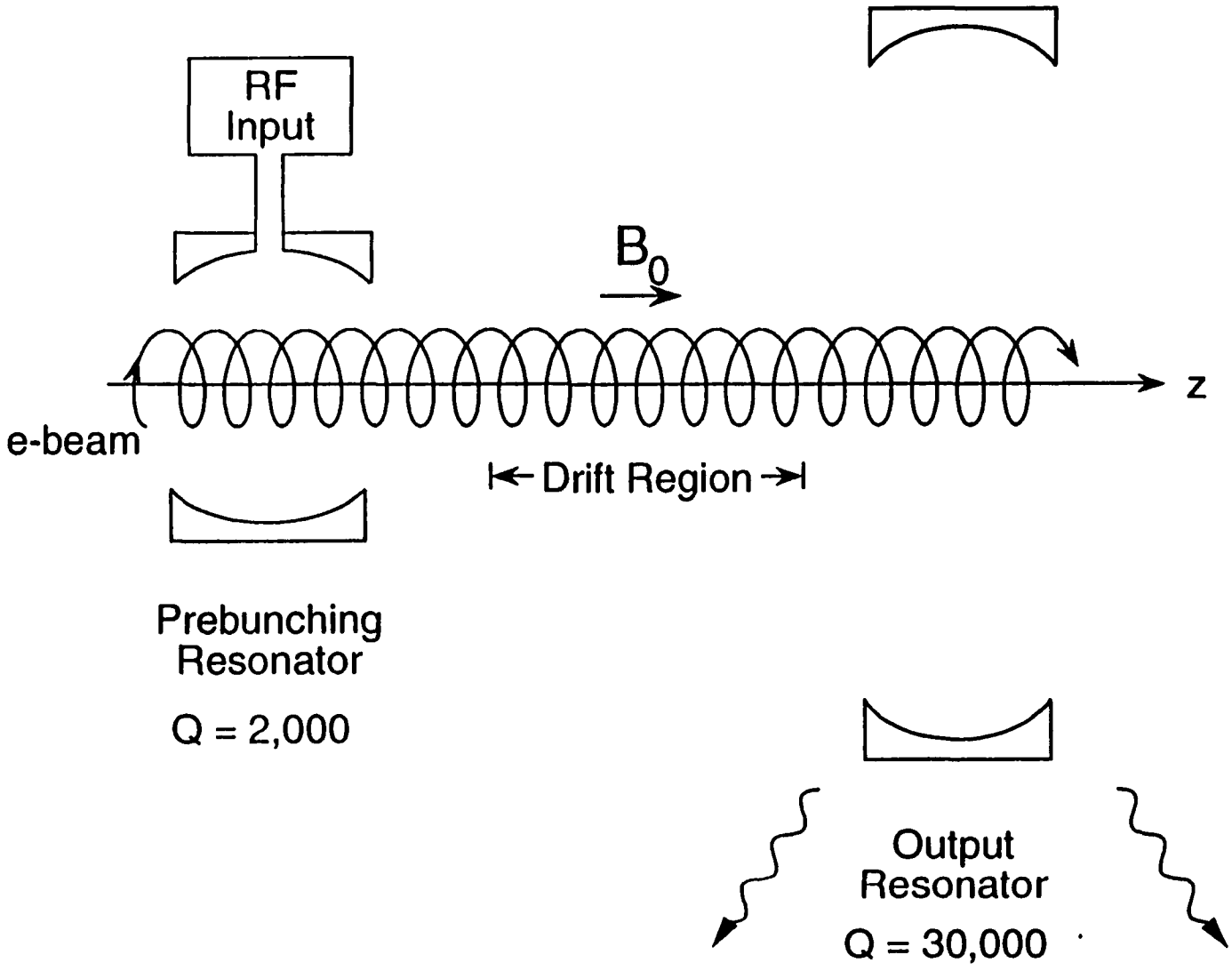

Fig. 1 Schematic of QOG with prebunching and output open resonators.

NRL Quasioptical Gyroklystron Experiment

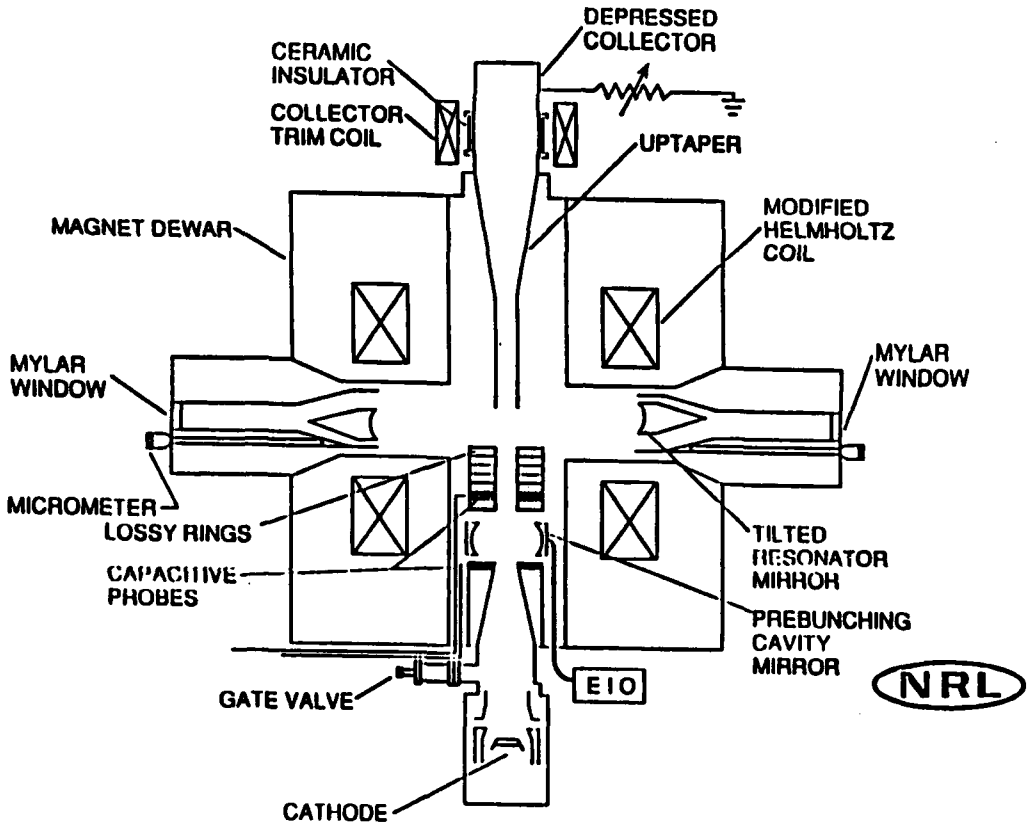

Fig. 2. Schematic diagram of the quasioptical gyroklystron experiment.

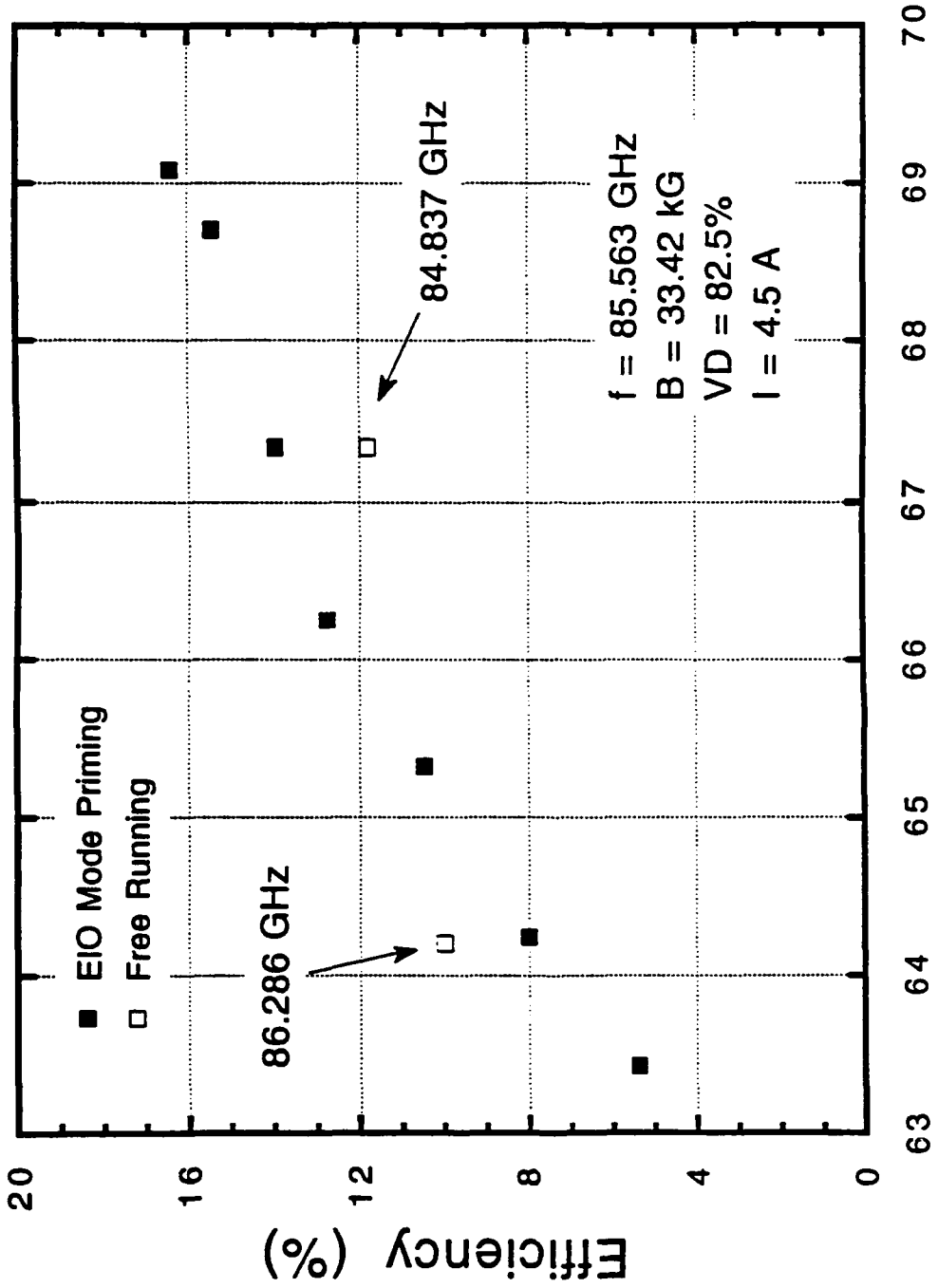

Fig. 3. EIO mode priming efficiency versus cathode voltage.

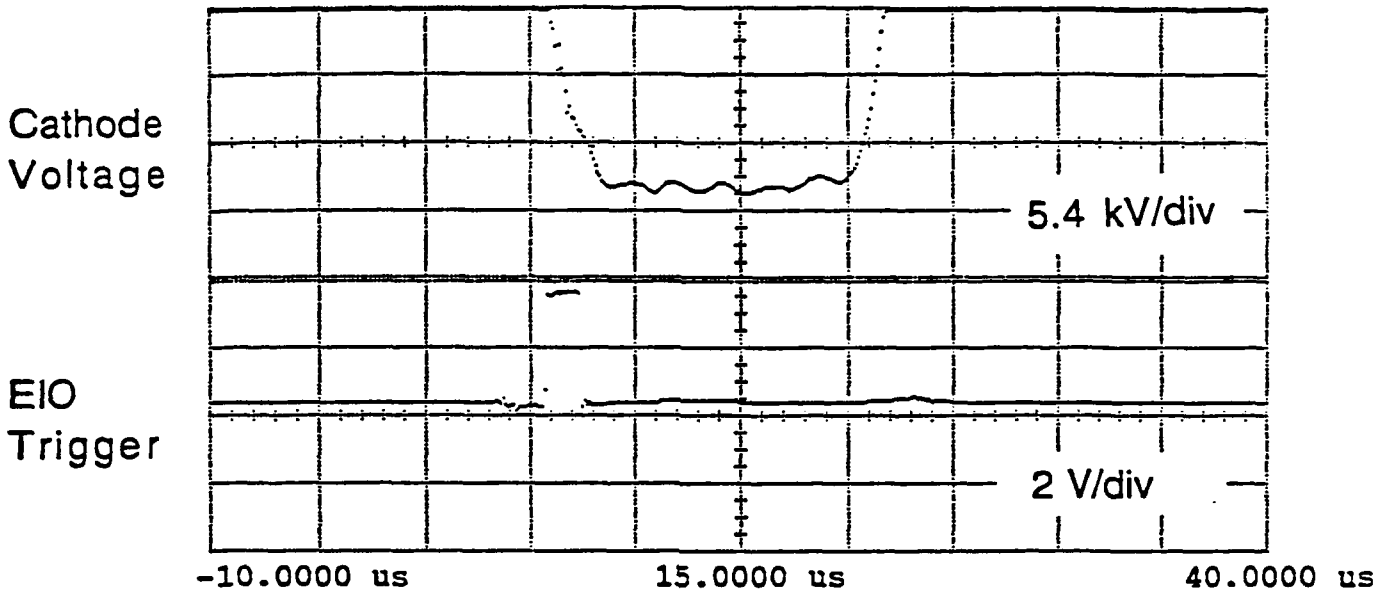

Fig. 4 The earliest the EIO can prime the gyroklystron.

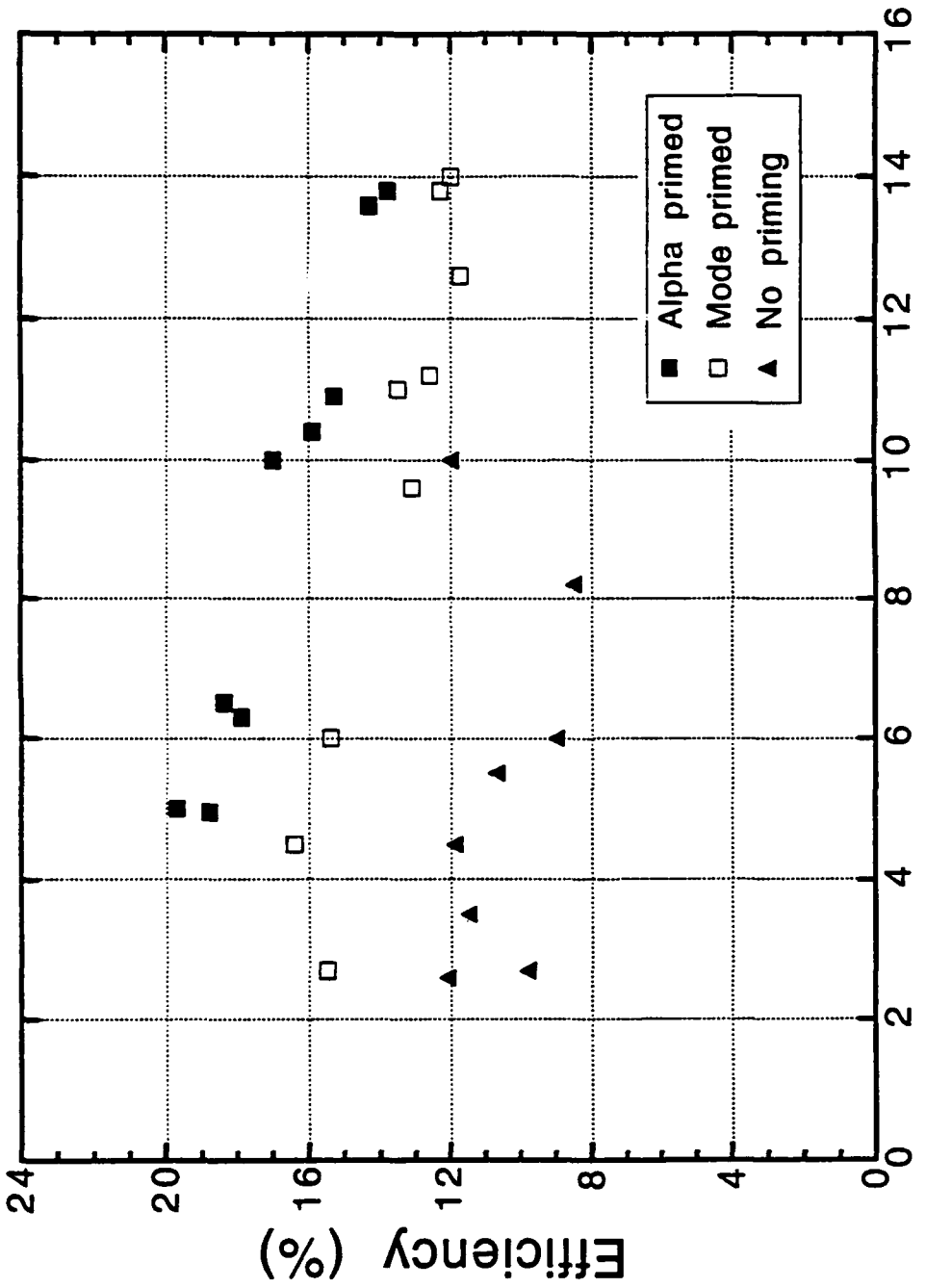

Fig. 5. Efficiency versus current for three regions of operation.

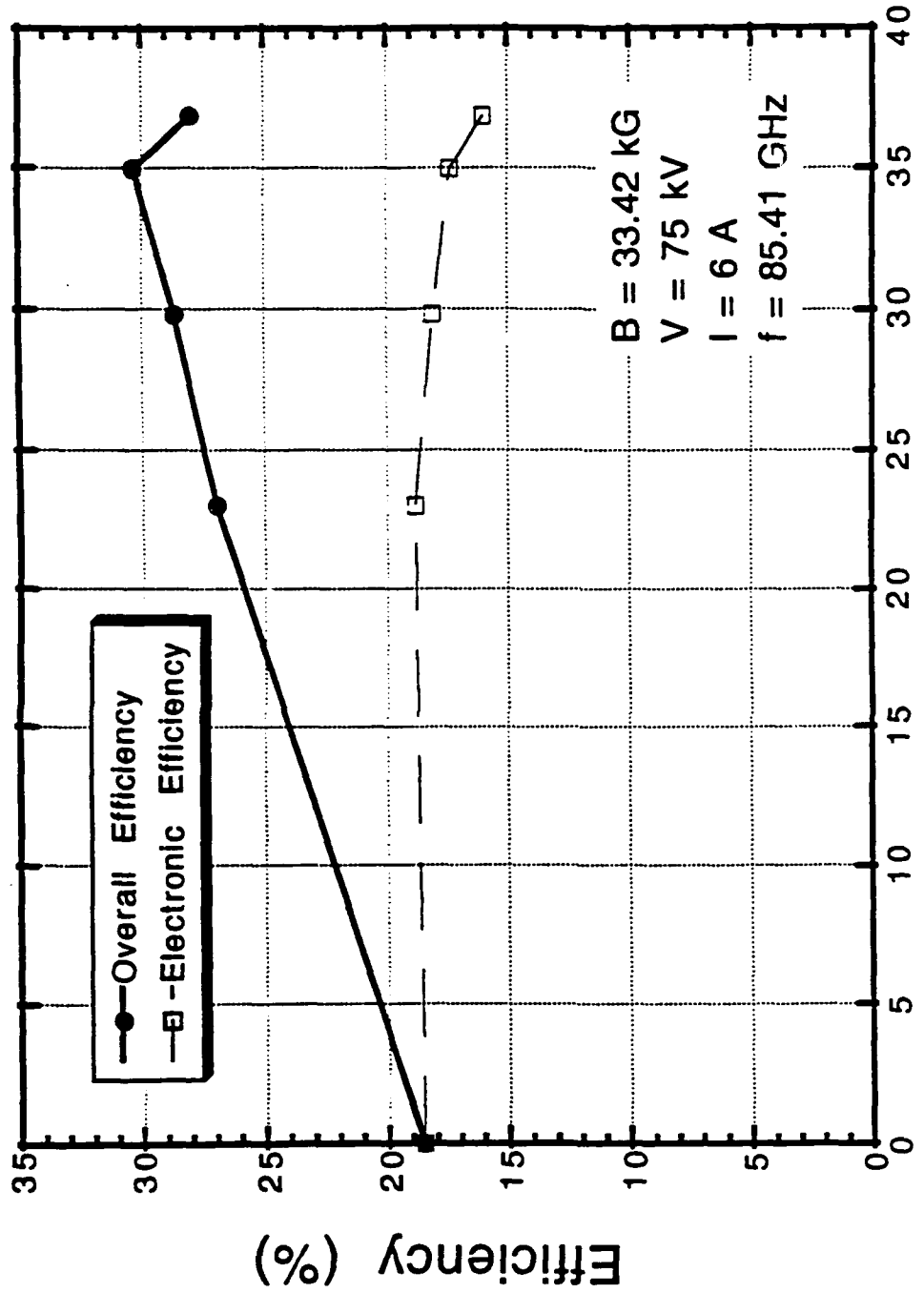

Fig. 6. Efficiency versus collector voltage depression for the gyroklystron.

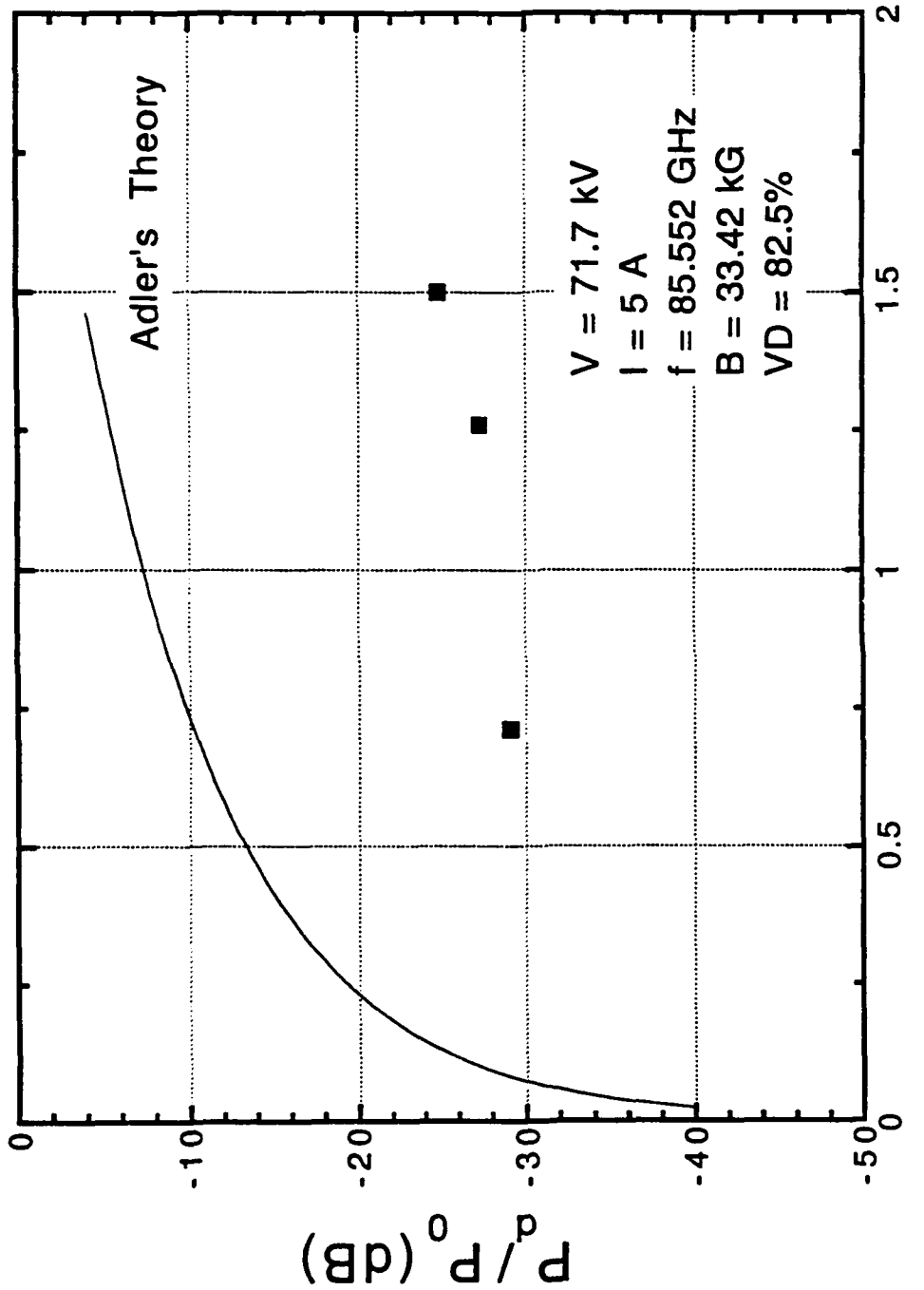

Fig. 7. EIO drive power versus phase-locking bandwidth.

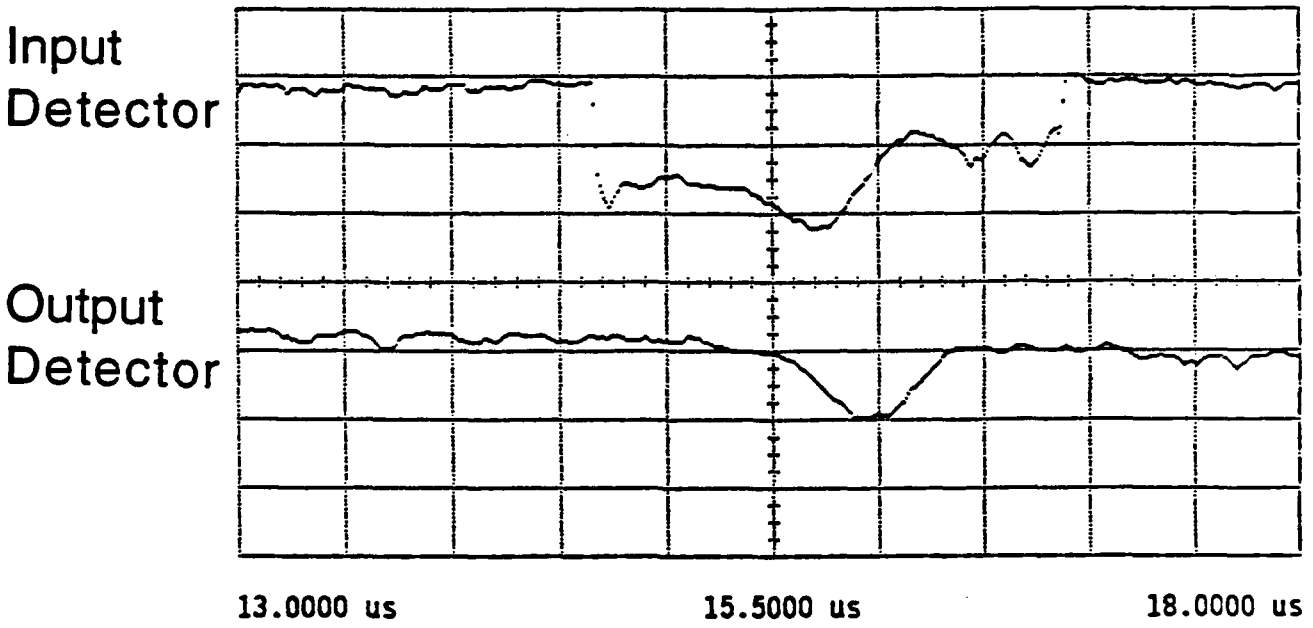

Fig. 8. Input and output signals during amplifier operation.

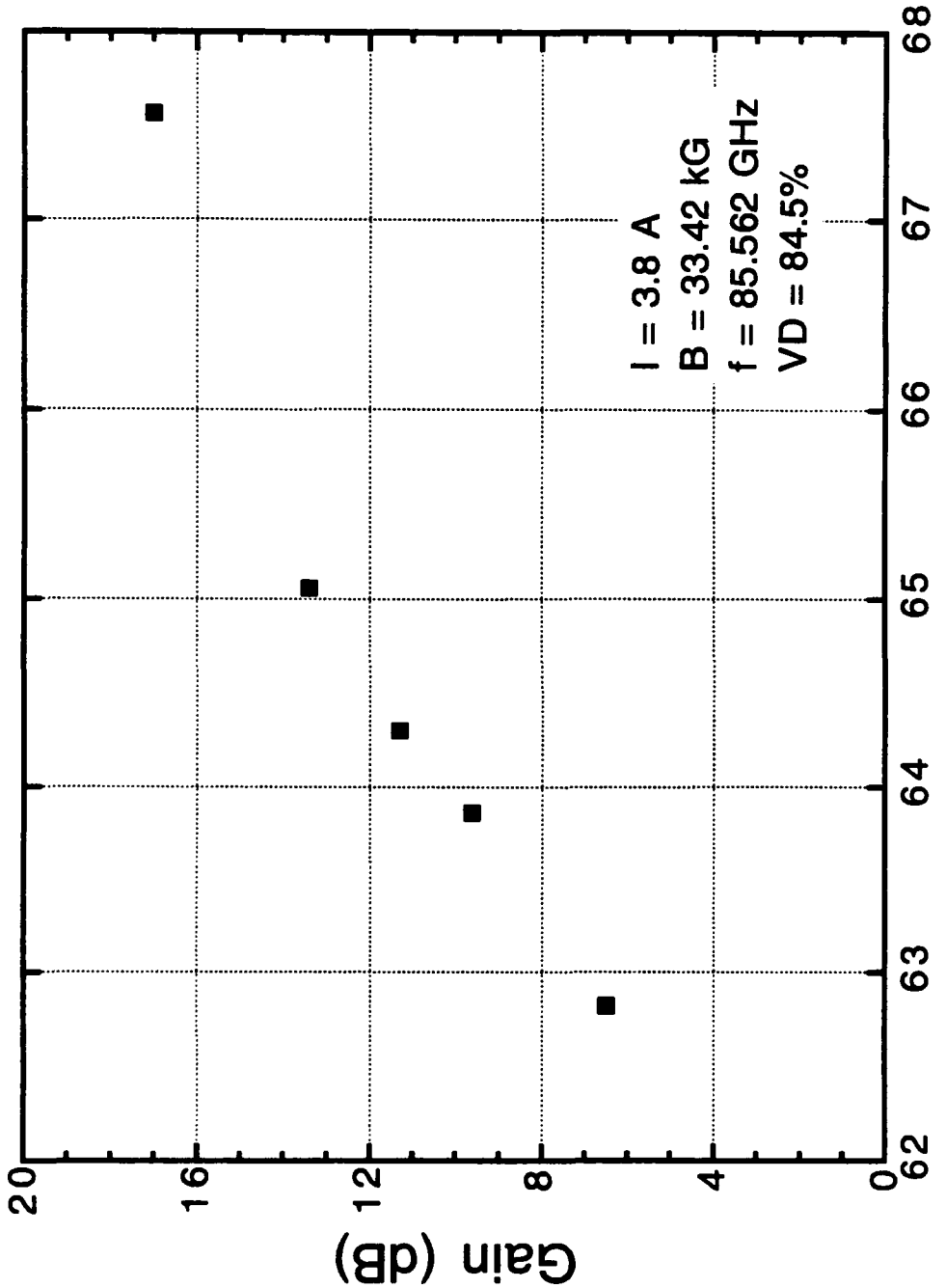

Fig. 9. Amplifier gain as a function of beam voltage.

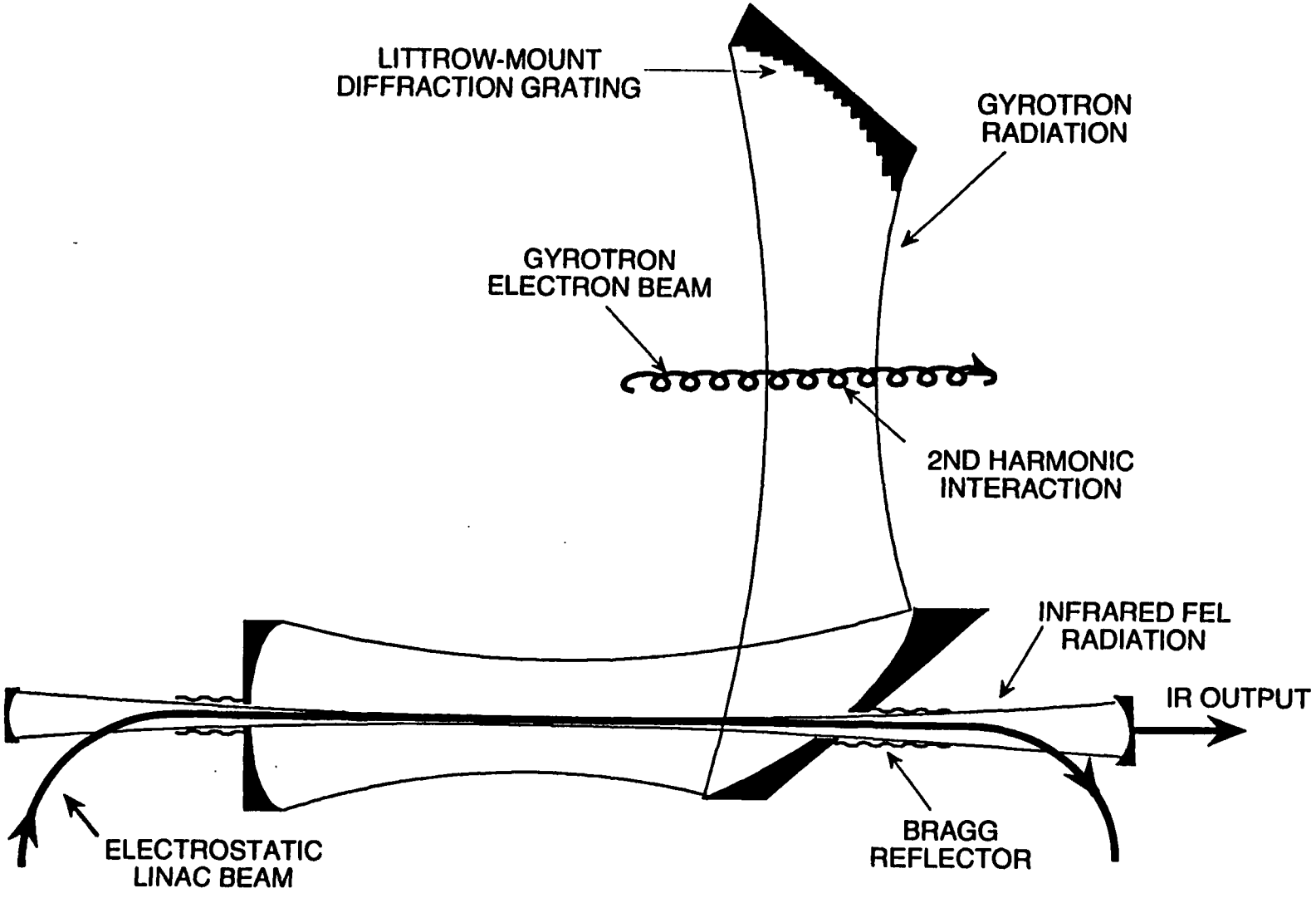

Fig. 10. Schematic of an IR FEL with a QOG-pumped electromagnetic wiggler showing the FEL beam path, sub-millimeter-wave QOG-wiggler resonator, and IR FEL resonator.

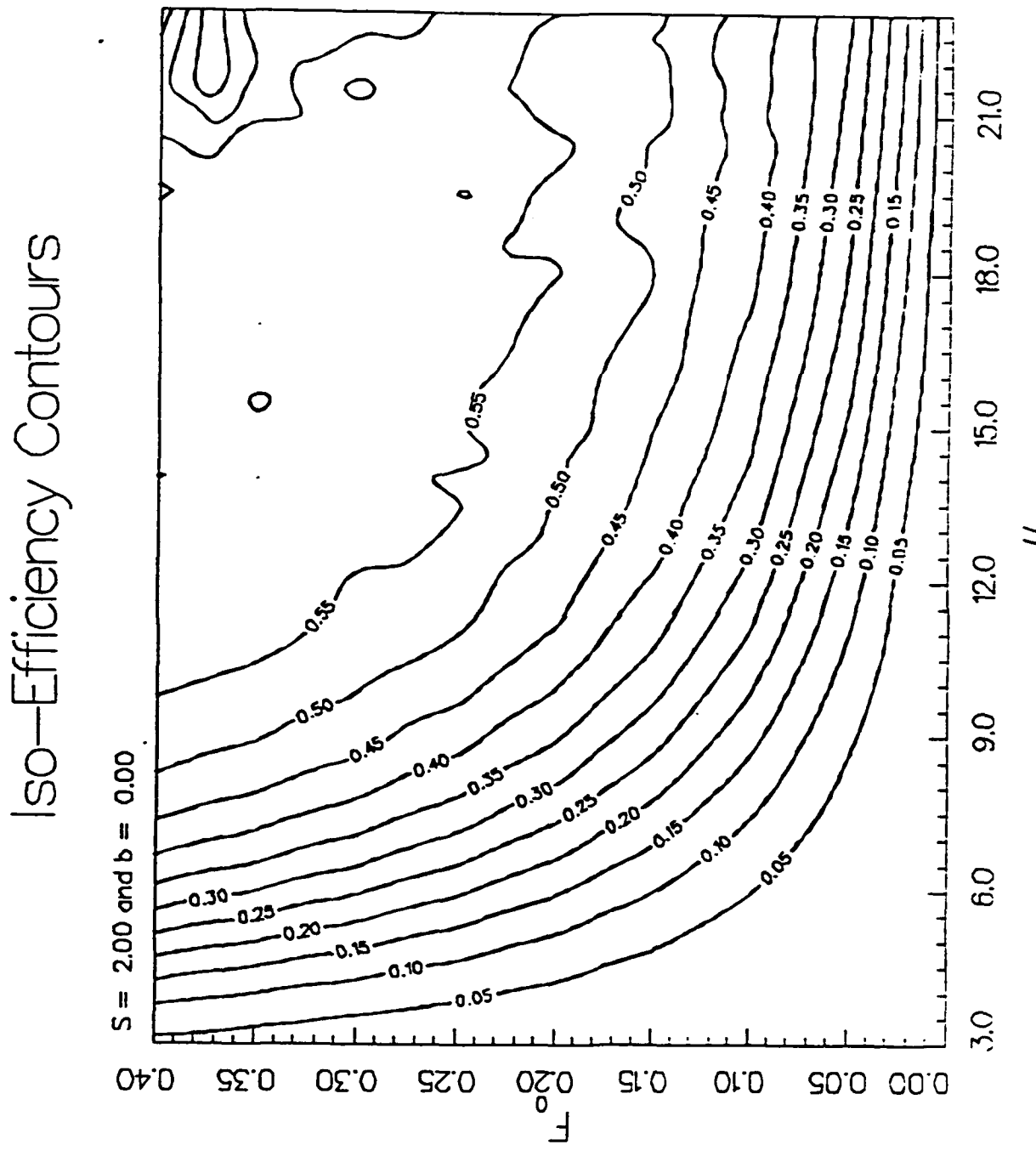

Fig. 11. Contours of normalized (transverse) efficiency as a function of normalized interaction length (μ) and normalized electric field amplitude (F_0) for the second harmonic QOG with a pencil electron beam.

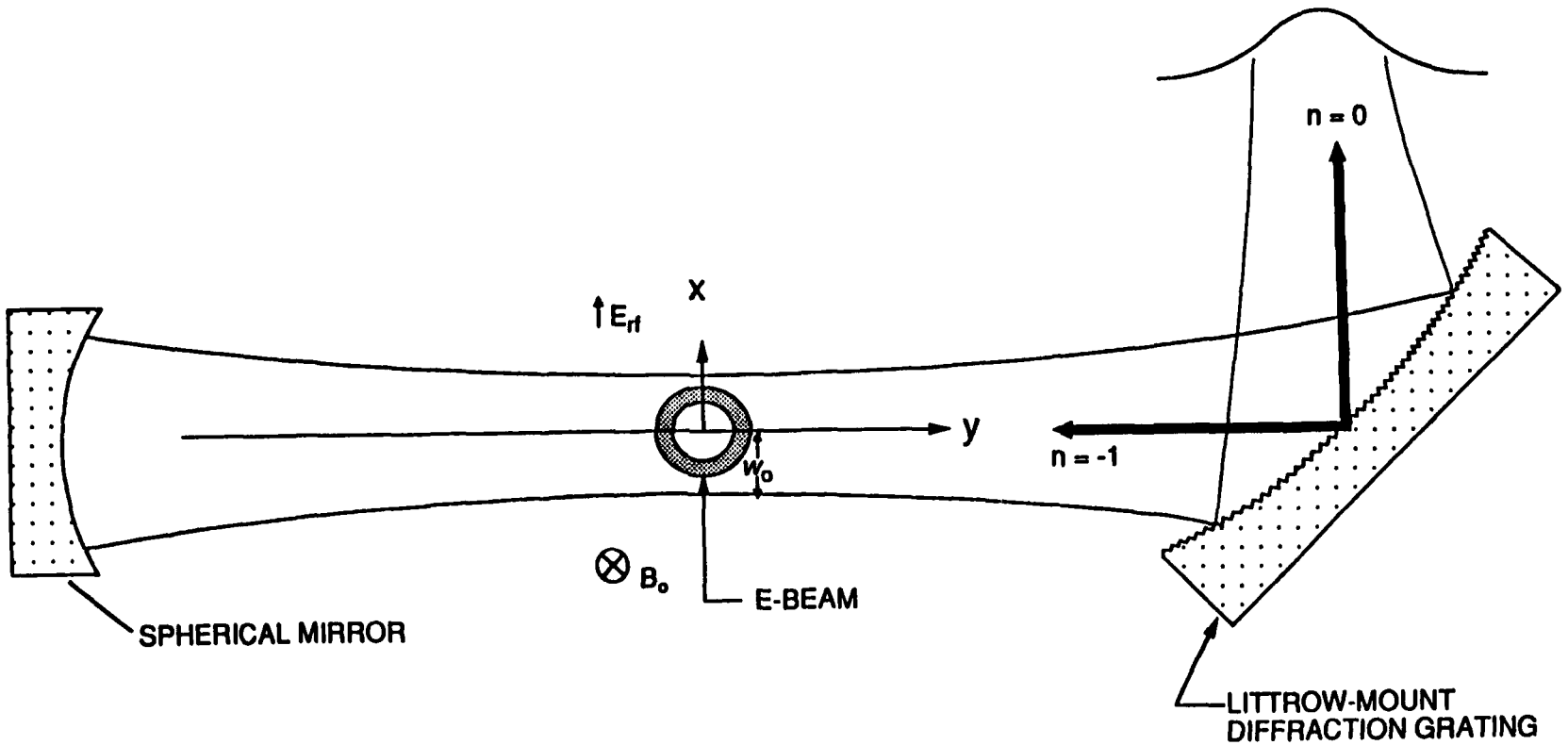

Fig. 12. Frequency selective resonator for the QOG based on a Littrow-mount diffraction grating.

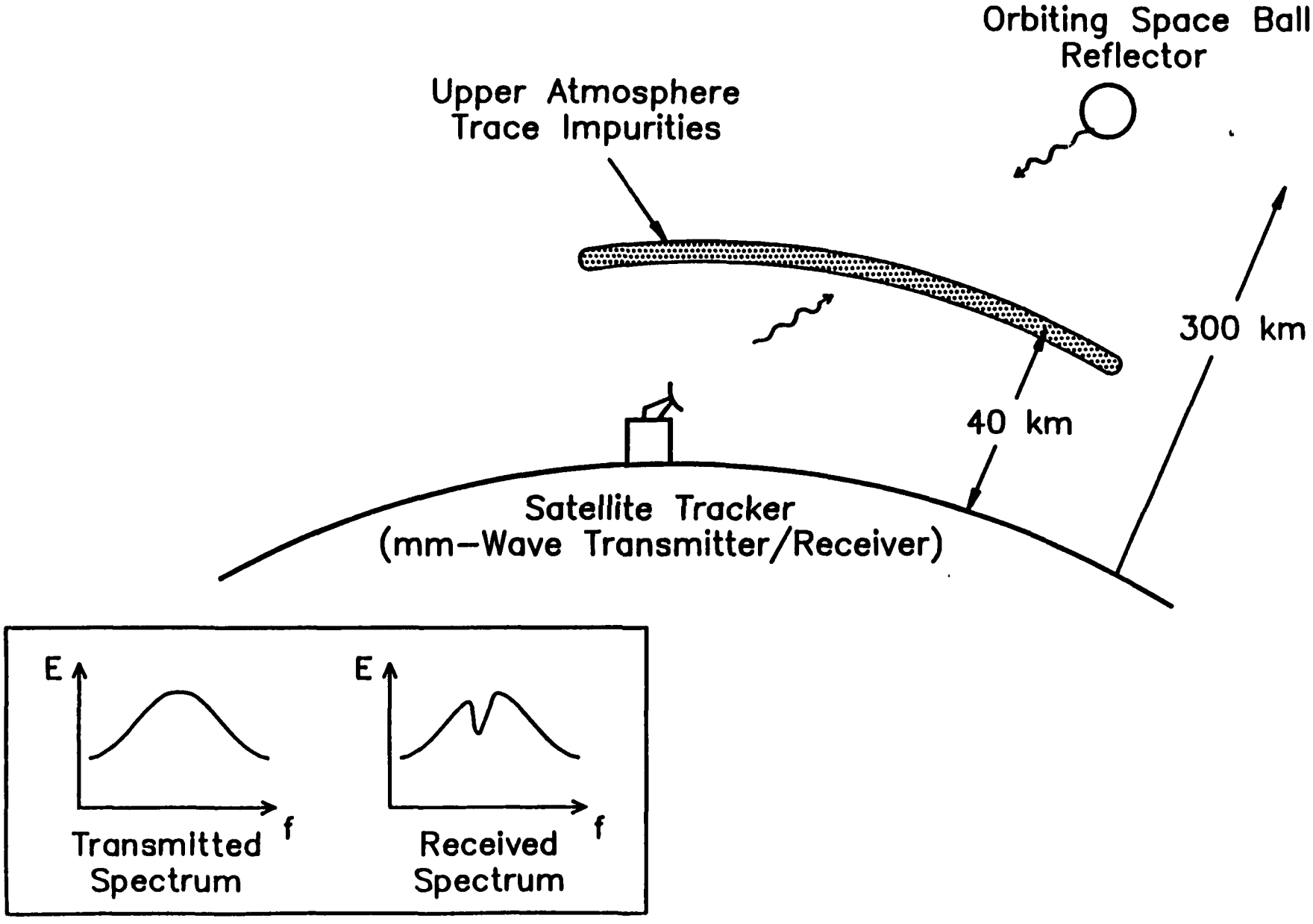

Fig. 13. Schematic of active sensor for detection of upper atmosphere trace impurities.